

UWS UNIVERSITY OF THE
WEST *of* SCOTLAND

SCHOOL OF ENGINEERING AND COMPUTING

**Optimal interior sound management for public
and individual transportation systems**

PHD THESIS

DANIEL SADRA, M.Sc.

Thesis submitted in fulfillment of the requirements
of the University of the West of Scotland
for the award of Doctor of Philosophy

*“You haven’t been born as a winner or a loser,
but as someone who has the choice”*

- Lou Holtz from 1937 -

Abstract

Due to cost intensive test set-ups, an alternative way to determine reliable absorption coefficients of surface wall materials is the use of simulation techniques. Obtaining accurate values of absorption coefficients meaning a deviation of 10% between simulated and measured absorption coefficients is crucial to enhance the quality of room acoustic simulations (ISO 10534-2, 2001). This means e.g. that simulated room impulse responses can be adapted to measured ones with a higher accuracy. In most cases, the absorption coefficients used in simulation models are measured under laboratory conditions using diffuse sound fields. In engineering applications, the interior sound field is excited by exterior noise in a specific frequency range. Due to vibro-acoustic coupling effects, the absorption characteristics of surface materials differ from those properties, which can be measured under ideal laboratory conditions. To optimize the characterization of surface wall absorption in purely room acoustic simulation – without vibro-acoustic modelling – an inverse identification approach based on ray tracing is proposed in this thesis. This approach requires initial values of absorption parameters, measured under laboratory conditions and room acoustic models of engineering applications, used to minimize the difference between the predictive model and measurements in the sound field. This PhD thesis proposes the application of such an inverse approach first validated with a theoretical model, secondly applied to a simple interior and finally tested in a generic aircraft cabin with a volume of $\sim 11\text{m}^3$. This mock-up is available at the University of Applied Sciences Hamburg and is comparable to a very light jet as one example for individual transportation. Furthermore, the enclosure is comparable to the one of a small bus which is used in public transport. To be able to apply the inverse approach, an acoustic simulation model has to be created. Therefore, several measurements have to be performed to identify the input parameters which are necessary to perform an acoustic simulation (e.g. absorption coefficients of the different materials, the directional characteristics of the loudspeakers). The energy decay curve is also measured in the enclosure, which should be simulated. In the next step, the initial values of the simulation model will be adapted using a least-square algorithm, until the energy decay curves from the acoustic simulation using ray-tracing are in accordance to each other. The results of this thesis show the suitability of the approach and give a first idea until which lower boundary the inverse method based on acoustic ray-tracing can be applied. A lower boundary of 1kHz could be identified when applied to the simple interior. For this generic problem, the room impulse responses has been reproduced ideally. For the application to the

very light jet, the inverse approach also provides a very good agreement of the absorption parameters above 1kHz (deviation below 5%). The reverberation time is underestimated by the simulation. The most relevant result of this thesis is that for the first time, such an inverse approach based on geometrical acoustics using ray-tracing has been successfully applied to a high complex, fully equipped generic aircraft cabin after the approach has been theoretically validated and tested in a simple interior with a low complexity. Moreover a lower boundary of 1kHz has been identified until this approach based on ray-tracing can be applied. With regards to the development of future interiors for public and individual transportation systems in the industry, this approach might lead to a cost-efficient development due to knowledge about the interior acoustics which can be transferred from available interiors in an early design stage. For public transportation systems, the approach has to be applied as well in future work.

Acknowledgement

It would not have been possible to write this master's thesis without the help and support of some people to whom I would like to give particular mention here.

Above all, I would like to express my deep gratitude to my supervisory team of this PhD thesis containing of Prof. Keshav Dahal, Dr. Pablo Casaseca-de-la-Higuera, Prof. Qi Wang and Professor Dr.-Ing. (habil.) Thomas Kletschkowski. Your patient guidance, enthusiastic encouragement and useful critiques throughout my thesis made this final thesis such a great experience for me.

Also I would like to recognize a colleague of the University of Applied Sciences staff Mr. Günter Willich who died in 2021 but has always been a faithful and long-term companion for my academic career.

I would also like to thank the Graduate Schools at University of Applied Sciences (Prof. Zita Schillmöller, Dr. Katrin Blankenburg and Inga Hesse) as well as the UWS (Gavin Morrison) for their help whenever need in various topics regarding this thesis.

I will also keep my two former colleagues Kenneth Hansen and Jens Hellemann in mind and the discussions we had during my supervision of their master thesis in 2015 Hellemann, J.: *Optimierung von Eingangsgrößen für raumakustische Simulationen unter Berücksichtigung inverser Methoden* and 2018 Hansen, K.: *Optimization of Simulation-based Predictions of Speech Intelligibility in Aircraft Cabins*.

My grateful thanks are also extended to my dear friends Dr. Florian Albrecht and Maximilian Schutzeichel who I shared an office at the university with and who were always interested about the progress I achieved and discussions which provided new input for the thesis.

Finally, I wish to thank my parents Bernhard and Monika Sadra for their support and encouragement throughout the period of this part-time PhD study.

Table of Contents

Abstract	II
Acknowledgement	IV
Table of Contents	V
List of Figures	VII
List of Tables	IX
List of Formula Symbols	X
List of Abbreviations	XIII
1 Introduction	15
1.1 Motivation	15
1.2 Problem statement	16
1.3 Development of Thesis objectives	18
1.4 Outline of Methodology	20
1.5 Outline of PhD thesis	21
1.6 Thesis contributions	21
2 State of the Art – Acoustic Simulation and Inverse Methods	23
2.1 Geometrical room acoustics	23
2.2 Modal room acoustics	24
2.3 Identification of research gap	26
3 Background – Room Acoustics and Measurement Techniques	29
3.1 Signals and systems in characterization of room acoustics	29
3.2 Basic formulation of acoustic parameters and impulse response measurements	35
3.2.1 Sound absorption	35
3.2.2 Sound scattering	37
3.2.3 Sound diffusion	38
3.3 Geometrical room acoustics for rectangular rooms	39
3.4 Experimental techniques in aircraft cabins	40
3.4.1 Measurement techniques of absorption properties	41
3.4.2 Measurement techniques used to determine the reverberation time	43
4 Methodology	46

4.1	Application of ray tracing as special case of geometrical room acoustics	46
4.1.1	Application of commercial acoustic software EASE.....	46
4.1.2	Self-designed software tool	47
4.2	Signal processing and data handling.....	49
5	Application of methodology / contributions	51
5.1	Simulation-based validation of inverse approach	51
5.1.1	Results of simulation-based validation of inverse approach	51
5.2	Simulation of real data – simple use case.....	53
5.2.1	Description of test-rig.....	53
5.2.2	Measurement technique and –chain.....	54
5.2.3	Results of simple use case.....	56
5.3	Simulation of real data - cabin mock-up.....	59
5.3.1	Description of test-rig	59
5.3.2	Measurement technique and –chain.....	62
5.3.3	Results of real data cabin mock-up.....	67
6	Conclusions & future outlook	74
	References.....	76
	Appendix A – Energy decay curves for semi-anechoic chamber.....	82
	Appendix B – Setup files absorption measurement.....	85
	Appendix C – Plots of Absorption Measurement in Mock-Up	87

List of Figures

Figure 1-1 V-process for system development lifecycle	17
Figure 3-1: Acoustic transmission path in a room as an LTI system, see (Vorländer, 2008).....	30
Figure 3-2: Schematic view of signal processing for direct convolution, see (ISO 18233, 2006).....	31
Figure 3-3: Schematic view of signal processing for spectral partition, see (ISO 18233, 2006).....	32
Figure 3-4: (a) Time representation of a sine sweep excitation signal and (b) time representation of the inverse filter corresponding to the sine sweep excitation signal, see (Farina, 2000)	34
Figure 3-5: Microflown devices for the in situ measurement of absorption coefficients	37
Figure 3-6: Comparison of different measurement approaches for the determination of absorption coefficients	42
Figure 4-1: Schematic functional diagram of RAPO (Hellemann, 2016)	48
Figure 4-2 Ray-tracing flow chart	50
Figure 5-1 simulation based validation of inverse approach for energy decay for receiver M4	52
Figure 5-2 simulation based validation of floor absorption	53
Figure 5-3 simulation based validation of wall absorption	53
Figure 5-4: acoustic simulation model of simple interior.....	54
Figure 5-5 Globe Source from Outline (https://www.outline.it/measurement/gsr/index.html [05/19/2021])	55
Figure 5-6: measurement chain for simple interior.....	55
Figure 5-7 Energy decay of M4	56
Figure 5-8 Reverberation time semi-anechoic room M1&M2	57
Figure 5-9 Reverberation time semi-anechoic room M3&M4.....	58
Figure 5-10 Absorption coefficients of semi-anechoic room	59
Figure 5-11 Mock-up Business Jet at HAW Hamburg	60
Figure 5-12 technical drawing of Mock-Up by Innovint Aircraft Interior GmbH.....	61
Figure 5-13 Cross-section of mock-up by Innovint Aircraft Interior GmbH	61
Figure 5-14 Acoustic Model (EASE) of business jet mock-up.....	62
Figure 5-15 Absorption coefficient of ceiling panel in mock-up.....	63
Figure 5-16 Ceiling panel absorption coefficients in EASE.....	64
Figure 5-17 Interior of Mock-up, rear end.....	64
Figure 5-18 Reverberation time T30 for mock-up	66
Figure 5-19 Averaged Reverberation Time Measurement (left) and Optimization (right)	67

Figure 5-20 Reverberation Time Measurement/Optimization for mock-up M1/M2.....	68
Figure 5-21 Reverberation Time Measurement/Optimization for mock-up M3/M4.....	68
Figure 5-22 Reverberation Time Measurement/Optimization for mock-up M5/M6.....	69
Figure 5-23 Reverberation Time Measurement/Optimization for mock-up M7/M8.....	69
Figure 5-24 Deviation Measurement-Optimization M1/M2.....	70
Figure 5-25 Deviation Measurement-Optimization M3/M4.....	70
Figure 5-26 Deviation Measurement-Optimization M5/M6.....	71
Figure 5-27 Deviation Measurement-Optimization M7/M8.....	71
Figure 5-28 Absorption ceiling panel & partition aft.....	72
Figure 5-29 Absorption sandwich panel & sidewall pax.....	72
Figure 5-30 Absorption seat backrest back & seat seating.....	73
Figure 5-31 Absorption seat backrest & carpet.....	73
Figure A-1 Energy decay curve M1.....	82
Figure A-2 Energy decay curve M2.....	83
Figure A-3 Energy decay curve M3.....	84
Figure B-1 Coefficient calibration of PU sensor.....	85
Figure B-2 Global Settings of Microflown Impedance gun measurement (1).....	85
Figure B-3 Global Settings of Microflown Impedance gun measurement (2).....	86
Figure C-1 Measured Absorption for sandwich panel.....	87
Figure C-2 Measured Absorption for partition aft.....	87
Figure C-3 Measured Absorption seat backrest back.....	88
Figure C-4 Measured Absorption for seat backrest.....	88
Figure C-5 Measured Absorption seat seating.....	89
Figure C-6 Measured Absorption carpet.....	89
Figure C-7 Measured Absorption sidewall pax.....	90

List of Tables

Table 2-1 Summary of literature review	27
Table 3-1: Overview of transformation of different signal types.....	31
Table 5-1 Measurement positions semi-anechoic chamber.....	54
Table 5-2 Absorption parameters used in acoustic simulation.....	63
Table 5-3 Microphone positions for reverberation time measurement.....	65

List of Formula Symbols

Greek letters

Symbol	Unit	Marking
χ	$[N/m^2]$	Bulk modulus
ω_1	$[Hz]$	initial radian frequency
ω_2	$[Hz]$	final radian frequency
ψ	$[^\circ]$	angle of incidence
ϕ	$[^\circ]$	receiver angle
Ξ	$[-]$	scattering coefficient
ϑ	$[^\circ]$	oblique angle
Π	$[dB]$	Sound power
ϕ	$[n / Hz]$	modal density
η	$[kg / s]$	damping loss factor

Latin letters

Symbol	Unit	Marking
\bar{A}	$[-]$	Average absorption coefficient
A_{spec}	$[-]$	Specular absorption coefficient
d_s	$[mm]$	Distance source-surface
d_m	$[mm]$	Distance microphone-surface
d_ψ	$[-]$	Diffusion coefficient
e	$[dB]$	Energy decay
e_0	$[dB]$	Initial energy
E_{spec}	$[dB]$	Specularly reflected energy
E_{total}	$[dB]$	Total Energy

f	$[Hz]$	Frequency
$h(t)$	$[Hz]$	Frequency impulse function
H	$[-]$	Transfer function
H_i	$[-]$	Transfer function of direct sound wave
H_r	$[-]$	Transfer function of reflected wave
k_r	$[-]$	geometrical spreading factor
L	$[dB]$	Sound pressure level
M	$[-]$	Matrix
n	$[-]$	number of receivers
P	$[Pa]$	Sound Pressure
P_T	$[Pa]$	Pressure test surface
P_F	$[Pa]$	Pressure flat surface
r	$[m]$	mean free path
R	$[-]$	Reflection coefficient
S_{xx}	$[W / Hz]$	Power spectral density
S_{xy}	$[W / Hz]$	Cross spectral density
t	$[s]$	time
T	$[s]$	Duration of time signal
U_n	$[m / s]$	Particle velocity under normal incidence
V	$[m^3]$	Volume of a room
$x(t)$	$[-]$	excitation signal
$y(t)$	$[-]$	room response
Z_n	$[kg / m^2 s]$	Impedance

Constants

Symbol	Value	Unit	Marking
c	340	$[m/s]$	Speed of sound at 20°C
p_0	$2 \cdot 10^{-5}$	$[Pa]$	Threshold of audibility
ρ_0	1,293	$[kg / m^3]$	Density of the medium at 20°C

List of Abbreviations

BEM	Boundary Element Method
BGN	Background Noise
CAA	Civil Aviation Authority
CLS	Coupling Loss Factor
CSD	Cross Spectral Density
DLR	German Aerospace Center
DLF	Damping Loss Factor
EASE	Enhanced Acoustic Simulator for Engineers
EASERA	Electronic and Acoustic Evaluation and Response Analysis
ER	Early Reflection
FEM	Finite Element Method
FFT	Fast Fourier Transformation
FMM	Fast Multipole Methods
GRAS	Manufacturer for Microphones
HAW	Hochschule für Angewandte Wissenschaften (Hamburg University of Applied Sciences)
HCAT	Hamburg Center of Aviation Training
HEIM	Manufacturer for Measurement Equipment
IFFT	Inverse Fast Fourier Transformation
ISM	Image Source Method
IRS	Inverse Repeated Sequence
LS	Loudspeaker
LTI-System	linear time invariant system
MATLAB	MATlab LABoratory (Software for the calculation of complex mathematical problems)

MLS	Maximum Length Sequence
MOF	Modal Overlap Factor
NASA	National Aeronautics and Space Administration
PSD	Power Spectral Density
RAPO	Room Acoustic Property Optimizer
RASTI	RApid Speech Transmission Index
RT	Ray Tracing
SEA	Statistic Energy Analysis
SI	Speech Intelligibility
SNR	Signal-to-noise ratio
SPL	Sound Pressure Level
STI	Sound Transmission Index
TRL	Technical Readiness Level

1 Introduction

1.1 Motivation

Optimal acoustic design of aircraft cabins can significantly improve not only passengers' comfort, but also staff health & safety and emergency procedures by increasing speech intelligibility and lowering noise level. An accurate measurement of speech intelligibility based on the acoustic properties of the materials is thus important to optimize cabin design. For speech intelligibility, the regulations for aircraft public address systems are defined by the civil aviation authority (CAA). Speech Intelligibility (SI) is expressed by the Speech Transmission Index (STI) or the RAPid Speech Transmission Index (RASTI) which are described in the standard IEC 60268-16 (IEC 60268-16, 2011). STI is defined using a scale from 0 to 1, based on weighted contributions from a range of frequency bands present in speech. Values larger than 0.6 STI define acceptable SI. The RASTI value depends on (a) the impulse response of the room, (b) the strength of the source signal and (c) the background noise at the receiver position. Accurately measuring all these quantities is usually not feasible due to cost intensive flight tests and "flight test on ground" (Wandel & Scheel, 2016) using laboratory conditions close to flight conditions. An alternative feasible and affordable way to certify speech intelligibility for design purposes is the use of simulation techniques.

In order to properly estimate SI, room acoustic simulations need to incorporate precise values of material parameters. Only this way STI and RASTI can be accurately obtained. A change of 20 % in the reverberation time as a result of the room acoustic simulation results in a change of approximately 0.03 RASTI (for 15dB signal-to-noise ratio) (Sadra & Kletschkowski, 2016) . In most cases the absorption coefficients used in simulation models are measured under lab conditions with normal or diffuse induced sound fields (ISO 354, 2003; ISO 10534-1, 2001). In aircraft cabins the sound fields are dominated by exterior sound, entering the cabin via structure-borne transmission paths or airborne sound transmission paths (Hubbard, 1994). The resulting interior sound field is therefore not only dependent on the material properties of the inner wall surfaces, but also on the vibro-acoustic coupling effects in the different sound transmission paths. Typical transmission paths are the airborne path (direct sound input through the fuselage) and the structure-borne path (vibrations travel through the structure and are radiated into the cavity at other locations). Moreover, additional sources like loudspeakers can excite the cavity. The latter has impact in both the frequency band of excitation and the absorption behavior of the surface materials. Vibro-acoustic coupling is neglected in standard room acoustic simulation

approaches (Vorländer, 2008) in which the model boundary is given by the inner surface represented by the interior walls. This leads to improper simulations when applied to SI and RASTI estimations in aircraft cabins.

So there is a need to improve room acoustic simulations to be able to better estimate parameters characterizing speech intelligibility (STI, RASTI). On the one hand it is necessary to compute the interior sound field without vibro-acoustic coupling and without external sources. On the other hand it is necessary to use measurement data for absorption coefficients which has been measured under laboratory conditions including vibro-acoustic effects but which might differ from measurements which have been performed in the installation state.

The motivation of this work is based on the processing of this area of tension.

1.2 Problem statement

For the improvement of room acoustic simulations to better estimate speech intelligibility parameters like SII and RASTI, it is necessary to intervene in the development methodology in a targeted way, based on common principles of system development. One common approach in the system development lifecycle is the use of the V-model (see Figure 1-1) which is a graphical representation of the necessary steps to ensure a successful development of a product. The development process is divided into three main parts. On the left hand side one starts with the idea and the requirements. Towards the bottom, those requirements will be more detailed before they will be implemented into the system design. On the right hand side, the system design will then be tested towards the input requirements to reach the technical readiness of the product.

Figure 1-1 illustrates exemplarily this process for the development of a new aircraft cabin in the aviation industry. The formulas and graphic presented are explained in detail in section 4.1.2. With regards to optimal sound management inside of aircraft cabins, it is well known from the literature (Vorländer, 2008), that the material properties (e.g. absorption of materials) are one of the main drivers besides the output level of the loudspeaker system which are installed inside the cabin and external noise sources to define interior acoustics. If a new cabin design will be developed (also involving new materials and an unknown cabin layout of future aircraft concepts like blended wing body, new type of monuments for lavatories or galleys, different seat layouts for first/ business and economy class and different seat materials), acoustic simulations of the interior noise field are performed in the early stage of the design process.

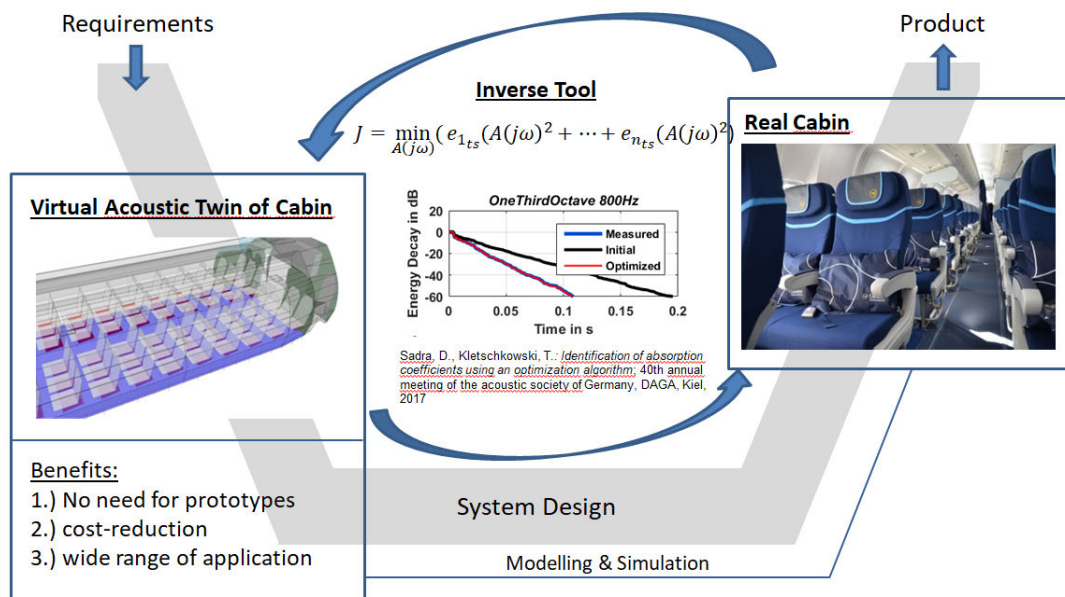


Figure 1-1 V-process for system development lifecycle

In order to close the gap between the virtual acoustic twin of the cabin and the real cabin, the question came up whether the application of inverse methods might help to improve the simulation quality of acoustic simulation models (virtual acoustic twin) in an early development stage. Inverse methods also known as backward calculations are commonly used if values for the boundaries are predefined and a solution for a certain point in the computational area can be found. The difficulty for problem in this PhD thesis is to infer boundary values (e.g. absorption coefficients) from measurement data inside the aircraft cabin.

In the future, the inverse approach (Knauber, et al., 2013) could also be used to transfer knowledge about existing interiors and sound fields to not only in the aviation industry, but for all kinds of public and individual transportation systems to reduce costs in the design process. The inverse tool as well as the cost-function is described in section 4.1.2.

The application of inverse methods in room acoustics is not new. In 2013 this method based on geometrical acoustics and ray-tracing was applied to identify absorption coefficients for a highly simplified room acoustic model (Pelzer & Vorländer, 2013). The necessary room acoustic measurements were performed with small volumes and without any seating or obstacles inside. It is not shown in detail if every absorption parameter of every surface was well matched after the inverse method was applied. However the paper provided a very good approximation for the energy decay of less than 10% deviation between measured and simulated energy decay curves.

So far this inverse method has been applied in the fields of room acoustics (e.g. concert halls), but not in environments like aircraft cabins, where the amount of acoustic parameters as well as the room acoustic are more complex (e.g. with regards to flexible lining structures in aircraft interiors instead of rigid walls in buildings).

1.3 Development of Thesis objectives

Research question: are inverse methods capable to identify parameters which increase the simulation accuracy of acoustic simulation models based on ray-tracing

General objective: enhance the prediction of room acoustic simulation by the application of inverse methods without the need of modelling external sources, sound transmission (airborne and structure borne sound) and vibro-acoustic

Sub-objectives:

- 1.) Further improvement of room acoustic simulation based on ray-tracing by the introduction of an inverse method based on acoustic quantities used to improve boundary conditions.
- 2.) Validation of further developed room acoustic simulation incorporating the use of inverse methods in a generic enclosure.
- 3.) Application of further developed method to realistic cabin environment.

In this thesis the term simulation is used. This means the combination of room acoustic calculations (application of ray-tracing) and an inverse method (used to improve the boundary conditions and the material properties).

At first, the basic idea of this research was to find an answer to the question how acoustic cavities have to be designed and excited to guarantee an optimal perception of sound at mid¹ and high frequencies. Sound management is mainly driven by the three factors: safety, comfort and privacy. All three of them have different requirements to the sound field. In a safety situation the perception of warning signals have to be ensured. It is not necessary to have a good quality of sound. Looking at comfort, a good reception of sound of announcements at high noise levels is essential. For privacy aspects, it is also necessary to have a good sound management inside the cavity. All three factors have to be ensured in a very early stage of the design process. Furthermore, sound management (especially speech

¹ Mid and high frequencies is always allocated to the ratio of wavelength and the dimension of the room. If the dimension is related to 1/10 of the wavelength, it becomes acoustically relevant.

intelligibility) is currently not a major design criterion (Pfeiffer, 2016) and is only benchmarked by performing experiments using prototypes (the interior design is already existing). Numerical simulation can be performed; however the implementation into the design process is small due to the fact that accepted validation processes are still not established. Especially the coupling to optimization problems is not exactly clarified at present. Also sufficient modelling of room acoustical problems involves a number of parameters (e.g. absorption coefficients, scattering coefficients) which are currently not easy to implement. The goal of research at that time was to formulate and solve an appropriate optimization problem based on objective acoustic quantities for optimal interior sound management in public and individual transport systems as well as to validate optimal solutions for Safety, Comfort and Privacy (SCP)-optimization with simplified experimental setups. Solving these problems will result in faster, cheaper and more efficient development of interior cabins. After having a good overview of the literature and intensive discussions, the question came up that talking about acoustic simulation the simulation sustainability is essential and how it can be improved. Even if it is possible to profit from knowledge of already designed interiors and make this knowledge usable for the design of new product development, the application of an inverse methods and the coupling to an optimization algorithm was the main part of the research. From acoustics it is well known that the energy decay and the reverberation time is an essential parameter for the characterization of an interior. Both are mainly driven by the absorption coefficient. (Knauber, et al., 2013) tried to use an inverse raytracing algorithm to optimize acoustic parameters. The research question came up whether it would be possible to perform such an inverse raytracing approach for cavities which are not square but cylindrical like an aircraft cabin. Another question is, if the optimizer is capable of handling the amount of absorption coefficients and still delivers acceptable results. When taking about the technical readiness level (TRL) (Mankins, 2004) which is defined as a measurement system which is used to assess the maturity level of a particular technology, this PhD thesis can be located at TRL 5 at the end. When a technology is at TRL 1, scientific research is beginning and those results are being translated into future research and development. TRL 2 occurs once the basic principles have been studied and practical applications can be applied to those initial findings. TRL 2 technology is very speculative, as there is little to no experimental proof of concept for the technology. When active research and design begin, a technology is elevated to TRL 3. Generally both analytical and laboratory studies are required at this level to see if a technology is viable and ready to proceed further through the development process. Often during TRL 3, a proof-of-concept

model is constructed. Once the proof-of-concept technology is ready, the technology advances to TRL 4. During TRL 4, the technology will be validated in laboratory environment. TRL 5 is a continuation of TRL 4, however, a technology that is at TRL 5 has to be tested in a relevant environment. Simulations should be run in environments that are as close to realistic as possible

1.4 Outline of Methodology

In this PhD thesis, an alternative way for determining the acoustical absorption coefficients of materials by using an inverse ray-tracing algorithm based on the measured energy decay is proposed.

The research can be divided into three main contributions to solve the objectives described in section 1.3. In a first step, the inverse method was applied to a simple room geometry. Here, two different simulation outputs regarding the energy decay of the room were the input data to the optimization algorithm to find the absorption coefficients of the surfaces inside the room. The amount of different materials was limited to three. This is used as the validation to see whether the optimization routine in Matlab which is used as the postprocessor was able to handle the data. In a second step, one dataset of the simple interior is replaced by real measurement data for the absorption of the different surface materials. The measurement of the energy decay was performed using a globe source and four different microphone positions.

In the final step of this research the inverse method was applied to a business jet mock-up at the University of Applied Sciences Hamburg. This mock-up was built by the *Innovint Aircraft Interior GmbH* and donated to the laboratory of cabin and cabin systems. The acoustic simulation model was built according to technical drawings of the cabin and the energy decay was measured using the sound system which installed by Innovint, was used in advance for active noise control investigations in the past. The absorption parameters of the different materials were measured using the in-situ impedance gun by *Microflown Technologies* (described in section 3.2.1), so that the frequency dependent absorption could be implemented into the acoustic simulation model. Results are given and discussed.

Finally the future outlook indicates what has to be done in the future to increase the quality of the gained results even more.

1.5 Outline of PhD thesis

In the introductory chapter 1, the motivation, the problem statement and the development of the thesis objectives are described. Moreover, the methodology which has been used is outlined. Finally, the contributions to this thesis are described.

Chapter 2 describes the state of the art. After an introduction into geometrical and modal room acoustics the results of the literature review are given. Here, the research gap was clearly identified for the application of inverse methods to complex geometries using ray-tracing as a method of geometrical room acoustics.

In chapter 3 the theoretical background on room acoustics and measurement techniques is discussed. At first, a short notice about the notation is made. Afterwards some basic information about general room acoustic problems and room acoustic simulations is provided. Finally an introduction into different measurement techniques for absorption coefficients as well as reverberation time is given.

Chapter 4 describes the methodology of the research.

Chapter 5 includes the application of the methodology. The three main steps (1) validation based on theoretical data (2) validation on simple geometry and (3) final application on more complex business mock-up model are illustrated and discussed before the conclusion and the future work which has to be done is discussed in chapter 6.

1.6 Thesis contributions

This research has been performed in the part-time PhD program at the University of the West of Scotland. Since the beginning in October 2014 the following contributions were achieved:

Contributions at the German Annual Conference on Acoustics:

SADRA, D.; KLETSCHKOWSKI, T.; *Identification of absorption parameters using an optimization algorithm*. DAGA 2017, 43th German Annual Conference on Acoustics (DAGA) Kiel, Germany, March 6-9, (2017)

SADRA, D.; KLETSCHKOWSKI, T.; *Optimal interior sound management for public and individual transportation systems: Evaluation of objective acoustic parameters*. DAGA 2016, 42th German Annual Conference on Acoustics (DAGA) Aachen, Germany, March 14-17, (2016)

Contributions at the University of the West of Scotland:

Best Poster Award – Annual Student Research conference in 2017 at the University of the West of Scotland. Best poster of PhD Student from Campus Paisley – School of Engineering and Computing

2 State of the Art – Acoustic Simulation and Inverse Methods

This chapter presents the relevant fundamentals regarding the state of the art in science and technology. These are the basics of the acoustic field calculation on the one hand and inverse methods based on the calculation methods on the other hand. The discussion shows where the gap in the state of the art is.

Simultaneous interior noise simulation in parallel to the design process has become an established procedure during the aircraft development process. Prediction models are created or derived from prior platforms (e.g. CAD – for geometry information) in order to predict the acoustic performance, to identify risks and to design the noise control for achievement of the top level aircraft requirements. In generic rooms the boundary conditions are defined and can be exactly controlled. In aircraft structures there are also vibro-acoustic coupling effects. This requires valid modelling approaches for the main aircraft structure (primary), the installation, cabin lining and systems (secondary) and the acoustic sources. There are two basic simulation approaches: First, a deterministic approach calculating the detailed wave propagation in the sub components of the aircraft and second, a random approach that determines the averaged energy of the wave in the subsystems (Pfeiffer, 2016).

Acoustic modelling of aircraft cabins is strongly dependent on which frequency range is selected for the investigation.

With an increasing frequency, normally FEM/BEM is used in the low frequency range. Geometrical acoustics such as ray-tracing are used in the mid frequency range whereas SEA is used in the high frequency range. [...]

2.1 Geometrical room acoustics

According to (Savioja, 2015), geometrical acoustics or the concepts of rays for modelling sound propagation are valid where the dimensions of a room and its reflecting surfaces are large compared to the considered wavelength of a sound wave (Kuttruff, 2009; Aretz, 2012). Sound rays can be considered as a small portion of a spherical wave with infinitesimal aperture which is transmitted from a certain source point and moves on a straight line with the speed of sound c under normal conditions. An impulsive signal from the sound source can thus be built as a point from which many sound rays are emitted at time $t = 0$. The reflected sound rays at room boundaries can be modelled by suitable specular or diffuse reflection laws, which are reflected back into the room with the loss of energy absorbed at the wall reflection. The room impulse response can be obtained from the source and reflection model by finding

the valid reflection paths on which sound rays that originate from the source at $t=0$ hit a designated receiver. Each of these reflection paths corresponds to a delayed impulse where its arrival time mostly depends on the path length and its amplitude and shape additionally depend on the absorption characteristics at the room boundaries, and the energy losses in the fluid medium. The sum of all reflections arriving after the direct sound is generally referred to as the reverberation of the room.

2.2 Modal room acoustics

Finite Element Method

According to (Zienkiewicz & Taylor, 2000) the finite element method (FEM) can be defined as a general discretization procedure of continuum problems posed by mathematically defined statements. The FEM is a method to solve field equations and first investigations took place in the 1960's (Thompson, 2006; Zienkiewicz & Taylor, 2000; Clough, R.W., 1960). The most common application in acoustics is the modelling of time-harmonic sound fields, i.e. to find solutions for the Helmholtz equation (Rienstra & Hirschberg, 2004). It can also be used to model narrow-band sound fields. In the FEM, a certain volume of a room gets subdivided into small volumetric elements. Every grid point contributes to the resulting system of ordinary differential equations. With the use of the Galerkin Method (Thomé, 2006) it can be ensured that the individual solution of these equations are the sound pressures at these grid points (Zienkiewicz & Taylor, 2000). The solutions for the sound pressure are then used as weights in the interpolation of a set of basic functions to approximate the sound field. When the values at the grid points are combined, an approximation of the solution of the Helmholtz equation (Wu, et al., 2022) at any point can be obtained (Thompson, 2006). Complex room acoustics can be modelled accurately due to the fact that the space can be partitioned using cells having a different shape which is one big advantage of the FEM. To find good quality partitions of arbitrary domains is a problem of certain importance which means in practice that the number of unknowns is too large for the number of differential equations to be solved in a reasonable computational time (Mehre, et al., Fe. 2012). Although one might exploit the fact that the matrices that characterize the system are sparse in general, different methods can be used to directly solve or further simplify the model. This means for example, that the system is transferred to a domain where it can be represented by just a few eigenmodes. The eigenvalues for the transferred modes are the base to solve the system. The number of unknowns increases as the cube of the temporal frequency (Deines, et al., 2006) since the grid size must be smaller than the smallest wave-length to achieve accurate approximations. If

broadband solutions are needed, these have to be synthesized from the individual results at the frequency of interest. The limiting factor is the required discretization of the volume or the surface small enough for the reconstruction of the wave and phase at every point of the discretization domain. As a rule of thumb it is often proposed in the literature to have at least six nodes per wavelength in each spatial direction (Franck, 2007). This is the reason why (Hubbard, 1994) proposes that FEM is the best method to use below 200 Hz.

Boundary Element Method

The boundary element method (BEM) is closely related to FEM. BEM requires a linear problem since the fundamental solution must be superimposed whereas FEM can also be used if the problem is non-linear. BEM uses the Kirchhoff-Helmholtz integral (Tygel, et al., 1994) to effectively reduce the dimension of the problem by one (Vorländer, 2008; Kopuz & Nalar, 1995; Ali, et al., 1995). Therefore, to solve a 3D spatial problem, meshes of discrete 2D surface elements at the boundaries are required to extrapolate the sound field in the whole enclosure. The Kirchhoff-Helmholtz integral is formulated in a discrete form and solved using matrix algebra. Compared to the FEM, the application of the BEM reduces the Helmholtz problem to a non-linear eigenvalue problem. Normally the matrices which characterize the system are fully populated and have no particular structure. In addition, they are much smaller than the ones generated from the FEM. To help ease the problem, techniques have been developed to formulate equivalent or approximate systems that can be expressed as a linear algebraic eigenvalue problem (Ali, et al., 1995). In the 90's, research has been focused on combining fast multipole methods (FMM) with BEM. The application of the FMM-BEM resulted in a performance that scale as the square of the temporal frequency (Mehre, et al., Fe. 2012) which makes this method more applicable for large enclosures compared to the FEM but still too complex to allow real-time simulation for broadband acoustic scenes.

For investigations in higher frequency ranges, other methods than FEM or BEM are more suitable because the amount of elements needed to guarantee a good discretization increases significantly as well as the computational time.

Statistic Energy Analysis

In statistic energy analysis (SEA) a system comprising an assembly of components of different material properties and geometric forms is modelled as a network of coupled subsystems (Fahy & Gardoino, 2007). In comparison to FEM and BEM which can only be used for low modal orders, the SEA can be used for high frequency range problems. Here, the

behavior of the structure is stochastic which means that the statistics of the system have to be taken into consideration (Petrone, et al., 2019). The SEA method is able to evaluate the vibrational response at high frequencies and is commonly used to predict interactions between reverberant sound enclosures and resonant structures (Mohammed & Wang, 2016). Engineering applications of the SEA normally involve the analysis of all relevant transmission paths and a description of the power flow in a connected subsystem through the Coupling Loss Factor (CLF) (Bouhaj, et al., 2017; Culla, et al., 2016). The successful application of SEA depends strongly upon the high modal density and the high modal overlap of the structure under investigation to ensure good average modal densities (Fareed, et al., 2001). The modal density can be precisely determined by using experimental modal analysis. The modal overlap factor (MOF) (Deines, et al., 2006) is a parameter which gives an approximate limit for the calculation of the vibro-acoustics and is calculated as follows (Eq. [2-1]):

$$\text{MOF} = \phi \eta f . \quad [2-1]$$

Where ϕ is the modal density, η the damping loss factor (DLF) and f the frequency. If the relation for $\text{MOF} < 1$ holds, FEM or BEM can be used. For $\text{MOF} > 1$, SEA should be used for reliable results (Fareed, et al., 2001; Kuttruff, 2009). The DLF of a given propagating wave can be defined as the ration between dissipated energy and total energy (Cordioli, et al., 2010). SEA is often used for the study of vibro-acoustic behavior of systems in the aeronautic, automotive and naval industry. The advantage of this method is the application in mid to high frequency ranges for investigations, the reduced computational time compared to FEM and BEM and less modelling effort of sources of noise and vibration. As SEA is a statistical method, the provided results are associated with average values in time space and in a combination of subsystems. In contrast to FEM/BEM - SEA gives integral values where no special discretization or local information is available. Some additional information can be found in (Lyon & DeJong, 1995; Burrough, et al., 1997).

2.3 Identification of research gap

To identify the research gap, a systematic literature review has been performed. The main result of this literature review is given in Table 2-1. Here, the different calculation methods are shown and the application in the frequency range evaluated. Moreover, based on references from the literature, it is also evaluated if inverse methods have been applied using one of these methods for simple and complex geometries.

As previously written in the problem statement section 1.2 it is essential for the general understanding of this thesis to know what is meant by an inverse method. In Acoustics, a general distinction between direct and inverse methods is made. Direct methods - also known as forward calculation – are used, when the boundary conditions are known and the solution of the computation area is calculated by solving the Helmholtz equation. For inverse methods – also known as backwards calculation – the solution can only be found for a certain point in the computational area. From known parameters, the unknown parameters of the boundary shall be identified. Therefore, models are used, which describe the system. For this purpose, models describing the system (e.g. the Helmholtz equation) are used to determine the deviations between estimated and measured values.

Table 2-1 Summary of literature review

	Frequency range (low/mid)	Frequency range (high)	Local resolution	Inverse methods (simple geometry)	Inverse methods (complex geometry)
FEM	✓	-	✓	✓	✓
BEM	✓	-	✓	✓	✓
SEA	(✓)	✓	-	-	(✓)
Geometrical room acoustics	(-)	✓	✓	✓	-

(Pfeiffer, 2016) focusses on the interior noise of aircrafts. He indicates, that based on the frequency range, different simulation techniques have to be used. He also suggests ray-tracing as a method of geometrical acoustics but does not clearly state, in what frequency range this method is applicable. Especially no connection to an inverse approach is given. One application for a simple room geometry is described by (Pelzer & Vorländer, 2013). They applied an inverse approach to a simple laboratory environment. So far an inverse approach has not been applied to a complex structure like an aircraft cabin.

(Mallardo, et al., 2012) suggested an accelerated BEM approach for an aircraft cabin. In the conclusion they suggest an upper boundary for the application of the BEM method of 1000Hz. Inverse methods have been applied to simple geometries like a loudspeaker

(Morkholt & Jacobsen, 2004) or a section of an aircraft (Valdivia, et al., 2008) and even applied for complex geometries like complex aircraft cabins (Valdivia & Williams, 2006) (Williams, et al., 2005) and (Klos, et al., 2005).

(Kletschkowski, 2012) applied inverse methods based on room acoustics in FEM but applied these methods just in the lower frequency range. For the identification of noise sources in an aircraft fuselage structure an inverse method based on FEM has been applied by (Kletschkowski, et al., 2011). In 2017 researchers developed an SEA model for a large commercial business jet and proved, that the cabin noise can also be predicted using this method. They give an example for a part of the cabin for 5000 kHz. (Dande, et al., 2017).

The red circle in Table 2-1 indicates where this research improves the state of the art and where the research gap is located.

3 Background – Room Acoustics and Measurement Techniques

In the previous chapter, the state of the art was discussed. The following chapter contains the essential theoretical principles that are necessary for understanding this work. These include the fundamentals of signal and system theory as applied to the description of acoustic systems, the fundamentals of room acoustics and the fundamentals of acoustic measurement techniques required for this work. The basics of room acoustics touch on topics like scattering and diffraction, which are not relevant for this thesis. These have been included for a complete presentation.

According to (Nelson & Elliot, 1991) all quantities which are frequency dependent are marked with capital letters and the argument ($j\omega$). All quantities in the time domain are marked with small letters and the argument (t). Furthermore, $[]$ will be used as an indicator for a mathematical operation and $()$ for the indication of an argument. Mathematical equations are also marked with brackets for identification and referencing (e.g. [chapter, number of equation]).

3.1 Signals and systems in characterization of room acoustics

In room acoustics, the accurate measurement of the impulse response is of paramount importance, since many acoustical parameters such as reverberation time T_{60} or clarity C_{50} can be derived from it (Oppenheimer, et al., 1999). Under the assumption of a source and receiver, the acoustical space in which they are placed can be considered as a linear and time invariant (LTI-) system characterized by the impulse response $h(t)$.

According to (Nelson & Elliot, 1991) the transfer function is assuming stochastic signals in general. For practical applications like measurements this procedure is also applied for deterministic signals. However, if the input and output signals are harmonic, the frequency response is calculated by dividing the Fourier Transform of the output by the Fourier Transform of the input. In the Laplace domain the transfer function is a mathematical representation of the system whereas in the Fourier domain, the frequency response function represents a transfer behavior which has been evaluated using measures. However, in practical applications the term transfer function and frequency response function are not every time distinguished in a very strict manner.



Content redacted due to copyright restrictions

Figure 3-1: Acoustic transmission path in a room as an LTI system, see (Vorländer, 2008)

Based on the acoustic transmission path of the LTI system shown in Figure 3-1, the essential process of deconvolution to determine the room impulse response using two alternative methods are represented in Figure 3-2 and Figure 3-3. The complex frequency response function $H(j\omega)$ can be estimated either by direct deconvolution or by spectral division of the response spectrum by the excitation spectrum. The frequency response function can be derived from the cross spectral density (CSD) divided by the power spectral density (PSD), see Eq. [3-2], if the spectrum is not measured frequency line by frequency line. The room response $y(t)$ to an excitation signal $x(t)$ can be calculated in the time domain by the convolution integral using the room impulse response $h(t)$:

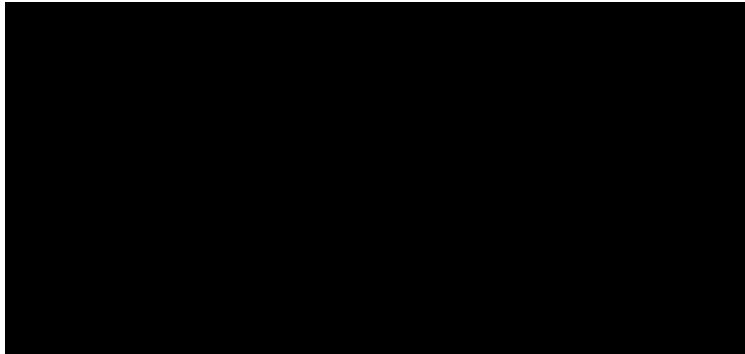
$$y(t) = \int_{-\infty}^{\infty} x(\tau)h(t-\tau)d\tau = x(t)*h(t) \quad [3-1]$$

or equivalently the frequency response function $H(j\omega)$ can be calculated by dividing the cross spectral density $S_{xy}(j\omega)$ by the power spectral density $S_{xx}(j\omega)$:

$$H(j\omega) = \frac{S_{xy}(j\omega)}{S_{xx}(j\omega)}. \quad [3-2]$$

In Figure 3-2, the deconvolution is performed by convolving the received signal together with the inverse of the excitation signal (ISO 18233, 2006). The inverse signal is the signal with the characteristic, that an ideal impulse is generated by convolution with the excitation signal. The impulse response deconvolution process is realized by linear convolution of the measured output with the inverse filter preprocessed from the excitation signal. Using linear convolution allows aliasing problems to be avoided. In fact, even if the time analysis window

has the same length as the emitted sine sweep signal (and is shorter than the impulse response to be measured), the tail of the system response may be lost, but this will not introduce aliasing.



Content redacted due to copyright restrictions

Figure 3-2: Schematic view of signal processing for direct convolution, see (ISO 18233, 2006)

The transformations between time and frequency domains are based on the Fourier Transform (FT) and its inverse (IFT) (Sevgi, 2007). The FT is valid for periodic and non-periodic time signals that satisfy certain conditions. The FT is defined for continuous time signals and in order to get the frequency domain representation, the time signal must be observed for an exact time window. Under these conditions the FT yields the frequency behavior of a time signal at every frequency with perfect frequency resolution (Sevgi, 2007). The Discrete Fourier Transform (DFT) is the discrete version of the FT that transforms time discrete signals from the time domain representation to its representation in the frequency domain with discrete frequency lines. The DFT is computationally expensive when the number of time samples is high. The Fast Fourier Transform (FFT) (Nelson & Elliot, 1991) is a faster computation of the DFT and provides significant performance advantages, even for a large number of samples if it is a power of 2. Table 3-1 gives an overview of the transformation of different signal types. The discrete frequency index is marked by (k) .

Table 3-1: Overview of transformation of different signal types

FT: continuous time to continuous frequency	$x(t) \rightarrow X(j\omega)$
FT of DS: discrete time to continuous frequency	$x(n) \rightarrow X(j\omega)$
DFT: discrete time to discrete frequency	$x(n) \rightarrow X(k)$
FFT: DFT in fast realization	
IFFT: inverse FFT	

The transformation between the time and frequency domain with the FFT is shown in Figure 3-3. After a transformation back into the time domain, using the Inverse Fast Fourier Transformation (IFFT) the impulse response is obtained.

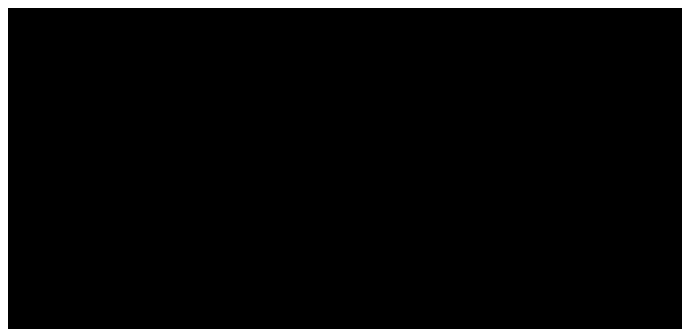
Two different ways to generate the transfer function can be used. In the first one, a circular convolution process relates the input and the output. The averaged output signal $y(n)$, derived from the time length of the FFT is used, if both the input and output signal are periodic. To obtain $h(n)$, the spectral ratio of output and input is transformed back to the time domain using the IFFT. Note that $h(n)$ is the discrete version of $h(t)$.

$$h(n) = IFFT \left[\frac{FFT[y(n)]}{FFT[x(n)]} \right]. \quad [3-3]$$

The other common approach is calculating the frequency response function $H(k)$ directly in the frequency domain by dividing the cross spectral density $S_{xy}(k)$ and the power spectral density $S_{xx}(k)$. The impulse response is then calculated by taking the IFFT from the result of this division:

$$h(n) = IFFT[H(k)] = IFFT \left[\frac{S_{xy}(k)}{S_{xx}(k)} \right]. \quad [3-4]$$

In both of the above approaches, due to the continuous repetition of the test signal and the fact that a circular deconvolution is performed, there is a risk of aliasing. This happens if the period of the repeated input signal is shorter than the duration of the system's impulse response $h(n)$ or the sampling rate in the time domain is lower than the Nyquist rate meaning that the sampling rate must be greater than twice the highest frequency of the time record.



Content redacted due to copyright restrictions

Figure 3-3: Schematic view of signal processing for spectral partition, see (ISO 18233, 2006)

With sine sweeps or chirps, a silence segment is commonly added after each signal, so that the time aliasing problem is avoided: if the data analysis window is still constrained to be of

the same length as the sweep, the last part of the tail can be lost, but it will not come back at the beginning of the deconvolved impulse response (appearing as noise before the arrival of the direct wave).

The impulse response obtained from broadband excitation is further processed to obtain the acoustic energy decay $e(t)$ for each octave sub-band of the calculating method with the so-called backwards Schroeder integral, defined as:

$$e(t) = \int_t^\infty h^2(t) dt = \int_0^\infty h^2(t) dt - \int_0^t h^2(t) dt . \quad [3-5]$$

The acoustic energy decay can be used for the characterization of an enclosure. It also indicates the damping of the room and the reverberation time can be derived from it.

The main properties defining the different excitation signals are described in Section 3.4.2. As one example, the Maximum Length Sequence (MLS) (Vorländer, 1996) technique can be used. The MLS technique is based on the excitation of the acoustical space by a periodic pseudo-random signal having almost the same stochastic properties as pure white noise. The number of samples in one period of an m order MLS signal is: $L = 2^m - 1$. MLS are generated, according to primitive polynomials, using digital feedback shift registers. Practically, the shift registers cycle through every possible binary values (or states) of the sequence (from this property came the notation maximum) with the exception of a vector with all zeros. The generation of polynomials $g(x)$ describing the combination of the register has the following form:

$$g(x) = x^m + a_{m-1}x^{m-1} + a_{m-2}x^{m-2} + \dots + a_2x^2 + a_1x + 1, \quad [3-6]$$

where $a_{1..m-1}$ is the weight (0 or 1) of the corresponding register unpin and $x^{0..m}$ is the value (0 or 1) of the register cell.

The Inverse Repeated Sequence (IRS) with a $2L$ samples period ($x[n]$) is defined from the corresponding MLS sequence of period L ($mls[n]$) by the following relation:

$$x[n] = \begin{cases} MLS[n], & \text{if } n \text{ is even, } 0 \leq n < 2L \\ -MLS[n], & \text{if } n \text{ is odd, } 0 < n < 2L \end{cases} . \quad [3-7]$$

The sine sweep technique developed by Farina (Farina, 2000) overcomes such limitations. It is based on the following idea: by using an exponential time-growing frequency sweep, it is possible to simultaneously de-convolve the linear impulse response of the system and to

selectively separate each impulse response corresponding to the harmonic distortion orders considered. The harmonic distortions appear prior to the linear impulse response.

In the logarithmic sine sweep technique, the excitation signal is generated on the basis of the following equation:

$$x(t) = \sin \left[\frac{T\omega_1}{\ln(\omega_2/\omega_1)} \cdot \exp \left(\frac{t}{T \ln(\omega_2/\omega_1)} \right) - 1 \right], \quad [3-8]$$

where ω_1 is the initial radian frequency and ω_2 is the final radian frequency of the sweep of duration T . Figure 3-4 shows the time representation of a logarithmic sweep and inverse filter with initial and final frequencies at 1 Hz and 50 Hz respectively.

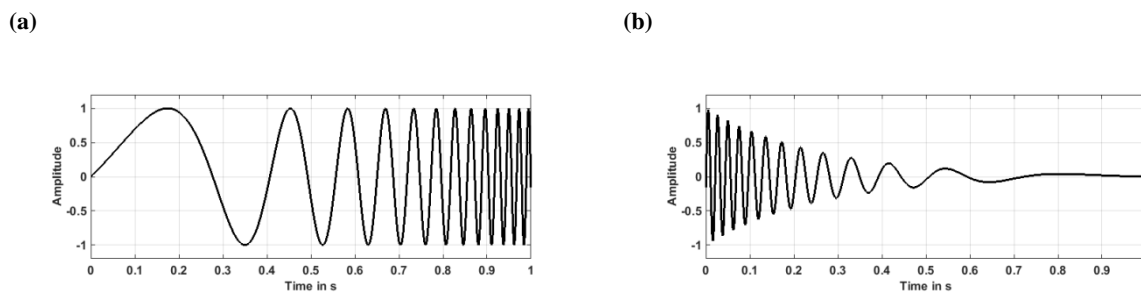


Figure 3-4: (a) Time representation of a sine sweep excitation signal and (b) time representation of the inverse filter corresponding to the sine sweep excitation signal, see (Farina, 2000)

In practice, an inverse filter $h_F(t)$ is constructed by time reversing the excitation signal. Then, convolving $x(t)$ with $h_F(t)$ gives the delayed Dirac delta function $\delta(t - \tau)$, see Eq. [3-9].

$$x * h_F = \delta(t - \tau) \quad [3-9]$$

The inverse filter can be described by:

$$h_F(t) = \frac{x(-t)}{\exp \left[\frac{t \ln(\omega_2/\omega_1)}{T} \right]}. \quad [3-10]$$

For the condition [3-9] the inverse filter has to have the behavior given in Figure 3-4. The signal energy has to be restricted if the signal described in Eq. [3-8] and the convolved with the inverse filter Eq. [3-10] should result in the Dirac impulse.

3.2 Basic formulation of acoustic parameters and impulse response measurements

3.2.1 Sound absorption

Characterization of room acoustic boundary conditions (Vorländer, 2008) is possible using the sound absorption coefficient $A(j\omega)$ which is defined as the ratio of the absorbed sound power $\Pi_a(j\omega)$ to the incident sound power $\Pi_i(j\omega)$.

The absorption coefficient can also be expressed as a function of the reflection factor $R(j\omega)$ by:

$$A(j\omega) = \frac{\Pi_a(j\omega)}{\Pi_i(j\omega)} = 1 - |R(j\omega)|^2. \quad [3-11]$$

The reflection factor $R(j\omega)$ is defined as the ratio between the complex amplitudes of the reflected $P_r(j\omega)$ and incident $P_i(j\omega)$ components of the sound wave, measured at the interface between the two media. This general definition of $R(j\omega)$ is valid for any sound field, $\Phi(j\omega)$ represents the phase for the complex representation.

$$R(j\omega) = |R(j\omega)| e^{j\Phi(j\omega)} = \frac{P_r(j\omega)}{P_i(j\omega)} = R_{\text{Re}}(j\omega) + j \cdot R_{\text{Im}}(j\omega) \quad [3-12]$$

Another quantity for describing wall properties is the impedance. The surface impedance $Z_n(j\omega)$ is defined as the ratio between the sound pressure $P(j\omega)$ and the particle velocity $U_n(j\omega)$ which is defined as $U_n(j\omega) = \vec{n} \cdot \vec{U}(j\omega)$, at the normal direction to the interface:

$$Z_n(j\omega) = \frac{P(j\omega)}{U_n(j\omega)}. \quad [3-13]$$

According to ISO 354 (ISO 354, 2003), the diffuse sound absorption, also known as Sabine absorption, is estimated in small/ large reverberation chambers by the following equation [3-14]:

$$A(j\omega) = \frac{55.3V}{S} \left[\frac{1}{T_s} - \frac{1}{T_0} \right] \quad [3-14]$$

where V and S are the volume of the reverberation chamber and the area of the sample. T_0 and T_s are respectively the reverberation times measured in the empty chamber and in the chamber with the sample. The ISO 10534-2 (ISO 10534-2, 2001) is based on the theory of the transfer function method for sound propagation in an impedance tube. For the two-microphone method (Bodén & Abom, 1986), the acoustic transfer function $H_{12}(j\omega)$ is calculated using the cross-spectrum of two microphones. The sound pressures $P_1^*(j\omega)$, defined as $P_1^*(j\omega) = \text{Re}(P_1) - j\text{Im}(P_1)$ and $P_2(j\omega)$, and the auto-spectrum of the first microphone:

$$H_{12}(j\omega) = \frac{S_{P_1 P_2}(j\omega)}{S_{P_1 P_1}(j\omega)}. \quad [3-15]$$

From this, the reflection coefficient can be rearranged as:

$$R(j\omega) = e^{i2kl} \frac{e^{ikd} - H_{12}(j\omega)}{H_{12}(j\omega) - e^{-ikd}}, \quad [3-16]$$

where k is the wave number, defined as $k = \omega/c$ and c being the speed of sound with 340 m/s, l is the distance from the sound source to the first microphone and d is the distance between the two microphones. The used sound absorption coefficient is obtained from equation [3-11]. The alternative methods, so-called in situ, rely on different techniques.

According to ISO 13472-1 (ISO 13472-1, 2004) the impulse method is defined by means of the ratio of power spectra between the incident and reflected sound pressure impulses, taking into account the geometrical spreading of sound waves:

$$A(j\omega) = 1 - Q_w(j\omega) = 1 - \frac{1}{k_r^2} \left| \frac{H_r(j\omega)}{H_i(j\omega)} \right|^2, \quad \text{with } k_r = \frac{d_s - d_m}{d_s + d_m} \quad [3-17]$$

Referring to Equation [3-17] $Q_w(j\omega)$ is the sound pressure reflection factor of the surface under test, k_r is a geometrical spreading factor including d_s as the distance source to surface under test and d_m as the distance microphone to surface under test, $H_r(j\omega)$ and $H_i(j\omega)$ are respectively the transfer functions of the reflected and direct sound waves. The in-situ method based on pressure-velocity relations uses the sound pressure $P(j\omega)$ and the particle velocity

$U_n(j\omega)$ to calculate the impedance $Z_n(j\omega)$, described in Equation [3-13]. From this, the sound absorption can be related with an incident plane wave under an oblique angle ϑ :

$$A(j\omega, \vartheta) = 1 - \left| \frac{Z_n(j\omega)/(\rho_0 c) \cos(\vartheta) - 1}{Z_n(j\omega)/(\rho_0 c) \cos(\vartheta) + 1} \right|^2, \quad [3-18]$$

where ρ_0 (1.293 kg/m^3) is the density and c the speed of sound of the medium at a temperature of $T_0 = 273,15 \text{ K}$ (0°C). The product $\rho_0 c$ is identified as acoustic impedance.



Figure 3-5: Microflown devices for the in situ measurement of absorption coefficients

The in situ impedance measurement device from Microflown Technologies (see Figure 3-5) has been used in this thesis to determine the starting values for the optimization algorithm described in Section 4.1.2). This device has also been used to measure the absorption coefficients in the business jet mock up described in 5.3.2.1.

3.2.2 Sound scattering

In room acoustic simulations, sound scattering describes how the energy of a sound ray which is emitted by a source behaves, after hitting the boundary layer of the acoustic model.

The energies of reflections (normalized with respect to a reflection from a rigid reference plane) are expressed as:

$$\begin{aligned} E_{\text{spec}}(j\omega) &= (1 - A(j\omega))(1 - \Xi(j\omega)) \equiv 1 - A_{\text{spec}}(j\omega), \\ E_{\text{total}}(j\omega) &= 1 - A(j\omega), \end{aligned} \quad [3-19]$$

where $\Xi(j\omega)$ is the scattering coefficient, $A(j\omega)$ is the incident absorption coefficient of the rough surface, $A_{\text{spec}}(j\omega)$ is the specular absorption coefficient of the smooth surface, $E_{\text{spec}}(j\omega)$ is the specularly reflected energy and $E_{\text{total}}(j\omega)$ is the total energy. The specular absorption coefficient is an apparent absorption coefficient since the energy may be scattered away from the specular reflection direction, rather than just being converted into non-acoustical energy. From these equations the scattering coefficient $\Xi(j\omega)$, according to ISO 17497-1 (ISO 17497-1, 2004) can be determined by:

$$\Xi(j\omega) = 1 - \frac{1 - A_{\text{spec}}(j\omega)}{1 - A(j\omega)} = \frac{A_{\text{spec}}(j\omega) - A(j\omega)}{1 - A(j\omega)}. \quad [3-20]$$

The specular absorption coefficient directly corresponds to the absorption coefficient if $\Xi(j\omega) = 0$. From the general definition in equation [3-20], several methods can be used to evaluate the scattering coefficient. All these methods differ in the way they separate the specular and the diffuse energy. The free field scattering coefficient (Eq. [3-21]) obtained from polar responses is obtained by correlating the scattered pressure polar responses from the test surface and a reference flat surface. This correlation scattering coefficient is given by:

$$\Xi_{\text{corr}}(j\omega) = 1 - \frac{\left| \sum_{i=1}^n P_T(j\omega, \varphi_i) P_F^*(j\omega, \varphi_i) \right|^2}{\sum_{i=1}^n |P_T(j\omega, \varphi_i)|^2 \sum_{i=1}^n |P_F(j\omega, \varphi_i)|^2}, \quad [3-21]$$

where $P_T(j\omega)$ is the pressure scattered from the test surface and $P_F(j\omega)$ is the pressure scattered from the flat surface, and φ_i the receiver angle of the i^{th} measurement position.

3.2.3 Sound diffusion

The diffusion coefficient is different from, but related to, the random incidence scattering coefficient. While the scattering coefficient is a rough measure that describes the degree of scattered sound, the diffusion coefficient describes the directional uniformity of the scattering, i.e. the quality of the diffusing surface (ISO 17497-2, 2016). ISO 17497-2 has favored the auto-correlation diffusion coefficient as being the most robust and useful measure. The diffusion coefficient d_ψ for a fixed source position can be calculated by:

$$d_\psi = \frac{\left(\sum_{i=1}^n 10^{L_i/10} \right)^2 - \sum_{i=1}^n \left(10^{L_i/10} \right)^2}{(n-1) \sum_{i=1}^n \left(10^{L_i/10} \right)^2} \approx \frac{\left(\sum_{i=1}^n 10^{L_i/10} \right)^2}{n \sum_{i=1}^n \left(10^{L_i/10} \right)^2}, \quad [3-22]$$

where L_i are a set of sound pressure levels in decibels, n is the number of receivers and ψ is the angle of incidence. This equation is valid when each receiver position samples the same solid reflection angle. The diffusion coefficient is intended to be evaluated either in a single plane or over a hemisphere.

3.3 Geometrical room acoustics for rectangular rooms

Under the simplifying assumption of a rectangular room (with room volume V) where only reflections at the boundaries take part, it can easily be shown that the average spacing between subsequent reflections arriving at a receiver is given by (Cremer & Müller, 1982) where t is the time and c the speed of sound (Eq. [3-24]):

$$\Delta t = \frac{V}{4\pi c^3 t^2}. \quad [3-23]$$

Consequently, the temporal energy decay in a room impulse response is only caused by the energy loss at the wall reflections and the propagation loss in the fluid medium. By further relating the average number of wall reflections after time t to the mean free path r in the room (Cremer & Müller, 1982) the following energy decay law can be derived:

$$e(t, j\omega) = e_0 \exp\left(-m_{air}ct + \frac{ct}{r} \ln(1 - \bar{A}(j\omega))\right), \quad \text{with } r = \frac{4V}{S}, \quad [3-24]$$

where e_0 is the initial energy at $t=0$, ct/r is the average number of wall reflections after time t , m_{air} is the absorption constant of the medium air, V is the room volume and S the room surface respectively. Furthermore \bar{A} is the average absorption coefficient of the walls for every single frequency. The sound field in the room must be sufficiently diffuse.

The basis of the inversion of the room acoustic ray tracing simulation algorithm is built by the energy histogram of Equation [3-26] and [3-27] (Pelzer & Vorländer, 2013). The energy portion of one ray in time that reaches the receiver depends on the initial energy e_0 and the energy loss according to the absorption and scattering coefficients of the walls that were reflecting this ray on the path from the source to the receiver.

$$e_{RT}(t, j\omega) = \sum_{p=1}^P e_{0,RT}(p) \prod_{i=1}^N (1 - A_i(j\omega))^{M_{pi}(j\omega, t/\Delta t)} e^{-m_{air}ct} \quad [3-25]$$

For a frequency ω , it uses the initial energy $E_{0,RT}$ of every ray p , the element of simulation matrix $M_{pi}(j\omega, t/\Delta t)$, where $t/\Delta t$ represents the correct time interval index at a time t . The matrix $\{M_{pi}\}$ includes all information about every emitted ray as well as information about distance, time delay, and which materials have been hit for every receiver position. Moreover, the frequency dependent absorption coefficient A_i of the i^{th} surface and the air absorption

$e^{-m_{air}ct}$ for the travel distance ct of the ray after a time t with the speed of sound c . (Pelzer & Vorländer, 2013). It is known that strong early reflections (ERs) are not modelled in ray tracing. Therefore, it can be beneficial to include the ERs matrix $\{M\}_{IS}$, which is calculated by the Image Source Model (ISM) similar to the ray tracing matrix $\{M_{pi}\}$ (Eq. [3-25]) into the energy decay. The contribution of $e_{IS}(t)$ of K image sources to the decay is calculated by [3-26]:

$$e_{IS}(t, j\omega) = \sum_{k=1}^K e_{0,IS}(p) \frac{1}{r_q^2} \prod_{i=1}^N [(1 - \Xi_i(j\omega))(1 - A_i(j\omega))]^{M_{pi,IS}(t/\Delta t)} e^{-m_{air}r_k} \quad [3-26]$$

In the ERs part, the spherical spreading $1/r$ must be taken into account for an image source with distance r , as well as the energy loss on the specular path due to sound scattering according to the frequency dependent scattering coefficients $\Xi_i(j\omega)$ for the i^{th} surface.

The results of [3-25] and [3-26] can afterwards be superimposed to calculate the total energy decay according to [3-27] (Pelzer & Vorländer, 2013):

$$e_{Total}(t, j\omega) = e_{RT}(t, j\omega) + e_{IS}(t, j\omega) \quad [3-27]$$

In ray tracing, these data represent the average absorption at random-incidence. Thus, in rooms that provide an approximate diffuse field, they serve well, particularly in the late response where in the region of high-order reflections, the average absorption coefficient is an appropriate quantity. The energy losses of the first reflections at their specific angles of incidence, however, are not accurately modelled. It should be kept in mind that the difference in energy loss at a specific angle of incidence to random-incidence may be up to 40 %, until the error of the reflection level exceeds 2 dB. Only at grazing incidence may the errors become larger. But at grazing incidence, anyway, other influences come into play (Vorländer, 2008).

3.4 Experimental techniques in aircraft cabins

For the determination of input variables (material properties and reverberation time) for the optimization algorithm which has been developed (see section 4.1.2) it is essential to have knowledge about experimental techniques for performing absorption as well as reverberation time measurements.

3.4.1 Measurement techniques of absorption properties

The employed methods to measure acoustical coefficients of materials in room acoustics focus on three main features of surface wall parameters: sound absorption, sound scattering and sound diffusion coefficients (see section 3.2). Common measurement methods to obtain sound absorption coefficients rely on normal or diffuse induced sound fields. The random incidence sound absorption coefficient, described in the ISO 354 standard (ISO 354, 2003), is a measure of the amount of incident sound that is absorbed. Diffusion is not an intrinsic property of the material, but it is caused by the room conditions. The standardized measurement method with normal induced sound field, ISO 10534-1/2 (ISO 10534-1, 2001; ISO 10534-2, 2001) uses an impedance tube. A distinction between the standing wave ratio and the transfer function method exists. A standing wave is a wave which oscillates in time with certain peak amplitude but with no movement in space. The main difference is that the standing wave technique uses one frequency at a time whereas the transfer function technique can measure the complete frequency range at once. Accuracy is obtained only for normal incident sound waves.

An alternative way for measuring sound absorption coefficients is the use of in situ techniques, described in (ISO 13472-1, 2004; ISO 13472-2, 2010; Kuipers, et al., 2012; Brandao, et al., 2015; Lanoye, et al., 2006). The in situ measurement methods allowing measurements in the real set-up, can be divided into two main groups; (1) those based on temporal separation of the incident and reflected sound pressures with the use of impulsive sound sources or signal processing techniques; and (2) those based on obtaining the surface impedance through the use of an algorithm, which is based on the mathematical formulation of the acoustic field. Both groups of methods are based either on the use of a single or a pair of microphones (or more in specific cases) or on the use of a probe that integrates a microphone and a particle velocity sensor, also known as pu-probe (de Bree, 2003). Accuracy is obtained for small angles of incidence for surface impedance $Z_n(j\omega)$ (Kuipers, et al., 2012). The application of the in-situ method is advised when the sound incidence is mainly normal or local plane waves can be assumed.

ISO 13472-2 (ISO 13472-2, 2010) describes a special in situ method based on an impedance tube which does not use special core samples. This method requires specific dimensions of the tube, microphone positions and in situ test fixture end piece, as specified below. The purpose of this standard is to measure on top of smooth reflective surface layers, where the

absorption does not exceed 0.15 (Wolkesson, 2013). Figure 3-6 compares three different measurement techniques. The in-situ method from the company Microflow (red line), the alpha cabin (a small reverberant room which is used for diffuse field absorption measurements) which has a diffuse field from 400 Hz onwards (blue line) and the impedance tube using two microphones (green lines). The absorption coefficients for a certain material from 400 Hz to 10 kHz have been measured and show deviations in different frequency bands. The Microflow device matches comparable measurements from the one of the suppliers using the impedance tube the best. The measurements in the alpha cabin and with the impedance tube have been part of a round robin test, where different samples have been tested by different companies. The measurement with the Microflow in-situ device has been performed in the laboratory. All measurement methods given in Figure 3-6 have different boundary conditions. The Microflow device measures in a real acoustic environment, not only under normal sound incidence.

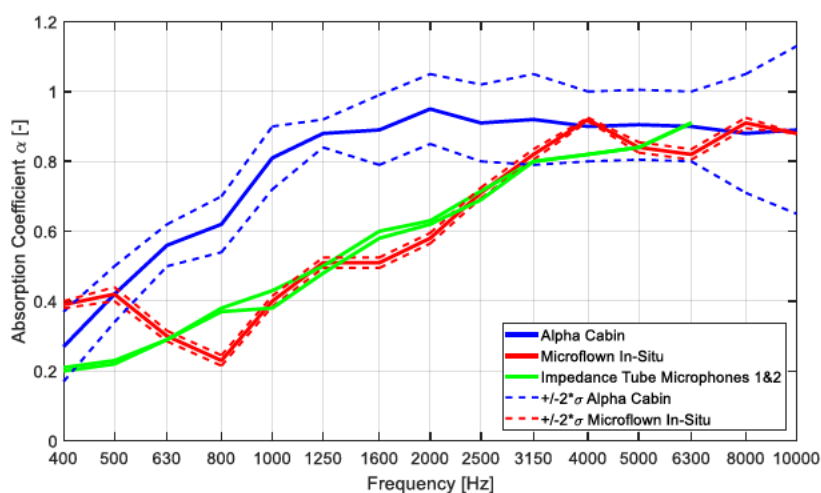


Figure 3-6: Comparison of different measurement approaches for the determination of absorption coefficients

The second important parameter in room acoustics characterization is the so-called scattering coefficient. The principle for measuring it consists in separating the reflected sound into specular and scattered components. The specular component is the proportion of energy which is reflected in the same way as would happen for a large plane surface (Ducourneau, et al., 2013). The scattered components provide the energy reflected in a non-specular manner. The scattering coefficient can be obtained from ISO 17497-1 (ISO 17497-1, 2004; Vorländer & Mommertz, 2000), using the rotating table method. Here samples are placed on a rotation table to measure the impulse responses (ISO 17497-1, 2004). Alternative methods were developed and identified as the correlation scattering coefficient and the specular zone scattering coefficient. The former calculates the cross-correlations of the polar response for a

scattering sample and a reference reflector. The latter, directly obtains the specular and total scattered energy from the polar responses (Cox, et al., 2006). The correlation scattering coefficient method has been presented by Mommertz and Vorländer (Mommertz & Vorländer, 1995) and is evaluated from polar responses in a free field, as a basis for the ISO standard.

Free field methods are often more laborious measurements to carry out, but can be readily predicted and are used to characterize the uniformity of scattering. The specular zone scattering coefficient (Vorländer & Mommertz, 2000) is calculated from the specular energy, by measuring the energy in the specular zone of a polar response. The total energy used can also be determined from the total energy under the polar response. Farina (Farina, 2000) applies a wave field synthesis approach to obtain scattering coefficients. This measurement is robust and requires little effort.

The diffusion coefficient, the last important parameter, is based on the Cox and D'Antonio technique (Cox & Lam, 1994; D'Antonio & Konnert, 1992) and builds the basis for the ISO 17497-2 (ISO 17497-2, 2016). This method evaluates the diffusion coefficient in a free field by measuring the uniformity of the reflected sound. The measurements are carried out using a boundary layer goniometer, in which 37 sequential impulse response measurements were made, using 37 fixed pressure zone microphones and a Maximum Length Sequence (MLS) excitation signal.

3.4.2 Measurement techniques used to determine the reverberation time

Reverberation time has always been one of the basic indicators of acoustic behavior (ISO 3382-2, 2008). Reverberation time is often used to describe the properties of the room behavior and is defined by the length of time required for the sound level to drop by 60 dB. Over the years, a number of different methods for measuring reverberation time have been developed and implemented. Common methods to obtain reverberation times from measurements are based on commonly used excitation signals, both deterministic and random. These methods are usually named after the type of employed signals:

- Interrupted noise.
- Maximum Length Sequence (MLS).
- Inverse Repeated Sequence (IRS) which uses a pseudo-random signal with white noise properties.

- Time-Stretched Pulses.
- Sine Sweep, which is based on time varying frequency signals.

The interrupted noise method, according to ISO 3382-2 (ISO 3382-2, 2008) is quite close to Sabine's original method. The room is acoustically excited using a wide-band signal. This method provides decay curves directly via the measured signal. However, the interrupted noise method does not provide an impulse response, only the reverberation time can be calculated from the energy decay. Other methods described in (Stan & Embrechts, 2016) for measuring the impulse response of such an acoustical space consist of applying a known input signal and measuring the system's output. A suitable excitation signal and deconvolution technique allow the impulse response to be obtained from the measured output, which is of essential importance. In terms of signal processing, the following points have to be kept in mind:

- (1) The emitted signal must be perfectly reproducible.
- (2) The excitation signal and deconvolution technique have to maximize the signal-to-noise ratio of the deconvolved impulse response.
- (3) The excitation signal and deconvolution technique must enable the elimination of non-linear artifacts in the deconvolved impulse response.

The acoustical impulse response measurements using the MLS technique were first proposed by Schroeder (Schroeder, 1979). The MLS technique is based on the excitation of the acoustical space by a periodic pseudo-random signal having almost the same stochastic properties as a pure white noise. MLS-signals have advantages in comparison to the unprocessed measurements. Because of the deterministic nature of the measurement signal, the measurement method allows maximum repeatability. The well-known problem of the MLS technique is the time-aliasing error. This error is significant if the length of one period is shorter than the length of the impulse response to be measured. Therefore, the order of the MLS sequence must be high enough to overcome the time-aliasing error.

The IRS technique was proposed as an alternative allowing a theoretical reduction of the distortion artifacts introduced by the MLS technique (Dunn & Hawksford, 1993). Aoshima introduced a new idea for the measurements of impulse responses which led to the time-stretched pulses technique (Aoshima, 1981). His idea was then pushed further by Suzuki et al. (Suzuki, et al., 1995) proposing what they called an "Optimum computer-generated pulse signal". The Time-Stretched Pulses technique is based on a time expansion and compression

technique applied to an impulsive signal (Suzuki, et al., 1995). The aim of using an expansion process for the excitation signal is to increase the amount of sound power emitted for a fixed magnitude of this signal and therefore to increase the signal-to-noise ratio without increasing the nonlinearities introduced by the measurement system. Once the response to this stretched signal has been measured, a compression filter is used in order to compensate for the induced stretching effects and to obtain the deconvolved impulse response. Farina (Farina, 2000) introduced the logarithmic sine sweep technique, standardized in ISO 18233 (ISO 18233, 2006) intended to overcome most of the limitations encountered in the other techniques. It is based on an exponential time-growing frequency sweep and is possible to simultaneously deconvolve the linear impulse response of the system and to selectively separate each impulse response corresponding to the harmonic distortion orders considered.

4 Methodology

In the following chapter, the methodology of this work will be presented, and both commercial software and self-developed software will be discussed. The data handling in connection with the cost function to be minimized is also presented.

4.1 Application of ray tracing as special case of geometrical room acoustics

As outlined in the state of the art, there are several problems regarding the use of FEM/BEM and acoustic simulation. Ray Acoustics Modeling belongs to the so-called geometrical acoustics solutions, see section 3.3. These solutions are very powerful because, as opposed to FEM or BEM solutions, their performance and accuracy is not mesh dependent. This means that the mesh should only capture the geometry, independently of the frequency we want to solve for. In addition, the geometrical solution is frequency independent which allows to extrapolate the results up to very high frequencies without substantially increasing the computational effort.

Geometrical acoustics (e.g. ray-tracing) have the advantage to model enclosures which does not have to be divided into subsystems. Moreover all types of surfaces can be implemented together with material data (e.g. absorption or scattering parameters). Geometrical acoustics also provide an advantage regarding computational time. The information in the resulting energy histogram can be converted into an impulse response used for auralization. The ray tracing approach is simple and easy to implement and can be easily scaled for accuracy by limiting the number of traced rays. If the position of the receiver is changed, the tracing of all rays needs to be redone (Deines, 2008). With regards to speech intelligibility investigations, ray-tracing and the computation of the STI as well as RASTI and STIPA is still commonly used in the industry.

4.1.1 Application of commercial acoustic software EASE

The Enhanced Acoustic Simulator for Engineers (EASE) suite is commercially available software which allows the creation of a 3D acoustic model and various possibilities for performing acoustic investigations such as computation of room impulse responses. Together with the AURA module being a highly sophisticated room-acoustic module, EASE is known as one of the most famous design software widely used by acoustic engineers all over the world (Ye & Fu, 2014). Other common tools for acoustic simulation are the commercial software ODEON or VA-One but these tools have not be part of these investigations. The AURA module which is integrated in the EASE software is based on the CAESAR software

which was developed by the RWTH Aachen. It can be considered as consisting of two different engines. One method is utilized for highly accurate auralization at selected receiver positions (AURA Response). The other one is less precise but much faster (50% savings in time) and therefore allows the calculation of many points (Aura Mapping).

When setting up an acoustic model, in general, geometrical data is entered or imported for CAD Software. In the next step, absorption parameters of the materials (walls/surfaces) are added. Material data, which has not been available, can be measured e.g. using the Microflown in situ impedance gun described in section 3.2.1. From this reverberation time and acoustic parameters can be computed. Finally loudspeakers can be added to the acoustic model. The 3D frequency response is provided by the manufacturer and part of the EASE database. If loudspeakers are not included in the database; the radiation characteristic has to be measured and implemented. Together with this data, complex impulse responses can be computed from any loudspeaker to any point in the room.

4.1.2 Self-designed software tool

The baseline version of the Room Acoustic Property Optimizer (RAPO) here presented was initially proposed in (Hellemann, 2016). The main goal of RAPO is to fit the energy decay of the simulation model to the measured one by adapting the absorption coefficients of the material parameters. The schematic functional diagram is given Figure 4-1. In the first version of RAPO (Hellemann, 2016) the optimization was based on a linear least-square fit. Due to the increase in input parameters (i.e. material parameters, number of source and receiver positions and complexity of the room) an enhanced version of RAPO (Sadra & Kletschkowski, 2017) was proposed including a non-linear least square fit.

The energy decay histograms of each source-receiver combination were fitted simultaneously for a certain time stamp t_{ts} to obtain more accurate absorption coefficient estimation (Knauber, et al., 2013). Each optimization run takes about 20 minutes (on a computer using an Intel i5 processor, 8 GB memory) to minimize the cost function (Eq. [4-1]) exemplarily for a certain $A(j\omega)$ for this complex test case:

$$\min_{A(j\omega)} \|e_{ts}(A(j\omega))\|_2^2 = \min_{A(j\omega)} (e_{ts}^2(A(j\omega)) + \dots + e_{nts}^2(A(j\omega))) \quad [4-1]$$

In Eq. [4-1], for every iteration 1 up to n, the cost function for the squared error of the energy decay e per time step ts dependent on the absorption coefficient $A(j\omega)$ will be minimized for

every available energy decay. A lower bound of $0.01 A(j\omega)$ and an upper bound of $1.01 A(j\omega)$ have been used for the optimization as a side condition. The optimization problem is convex. From different starting points the same result could be achieved, so the non-linear least squares solver (internal optimization routine in Matlab - LSQnonlin) is capable of finding the global minimum of the cost-function. After some mathematical reformulation of equation [3-24]:

$$\begin{aligned} \frac{e}{e_0} &= e^{\left(-mct + \frac{ct}{r} \ln(1-A)\right)} \\ &= e^{-mct} \cdot e^{\frac{ct}{r} \ln(1-A)} \\ &= e^{-mct} \cdot \left(e^{\ln(1-A)}\right)^{\frac{ct}{r}} \\ &= e^{-mct} \cdot (1-A)^{\frac{ct}{r}} \\ J &:= \left(\frac{e}{e_0}\right)^2 \\ J &\xrightarrow{A} \min \end{aligned}$$

one can notice, that the cost-function for the optimization is non-linear in A .



Content redacted due to copyright restrictions

Figure 4-1: Schematic functional diagram of RAPO (Hellemann, 2016)

Figure 4-1 shows the schematic functional diagram of RAPO. Here the user fits both inputs (simulated and measured energy decay) into the optimization algorithm to find the minimum of the cost function in a loop process. Initialization values for the set of parameters needed to obtain the absorption coefficients have to be available for the optimization routine. After every iteration the deviation between the measurement data input and the optimized energy decay based on the absorption coefficients is checked.

4.2 Signal processing and data handling

For this research EASE was used as the pre-processor. All the post processing was performed in Matlab. The geometry is modelled and the ray-tracing impact file will be calculated via a simulation in EASE. The following input files needed for the inverse approach and to start the optimization routine in Matlab:

- EASE Trace file (.dat format)
- EASE Material file (.xwm format)
- EASE Face file (.xfc format)
- File including measurement data (energy decay, reverberation time)
- Humidity, Pressure and Temperature can also be adapted to influence the damping of the air

The inverse approach basically operates in four different phases. First the input files have to be provided. Second simulation data will be processed. Third measurement data will be processed before the last phase, the optimization algorithm starts operating.

For the necessary ray-tracing simulation in EASE a flow chart is given in Figure 4-2. This general flow chart shows the decision matrix which will be taken into account while performing a ray tracing simulation.

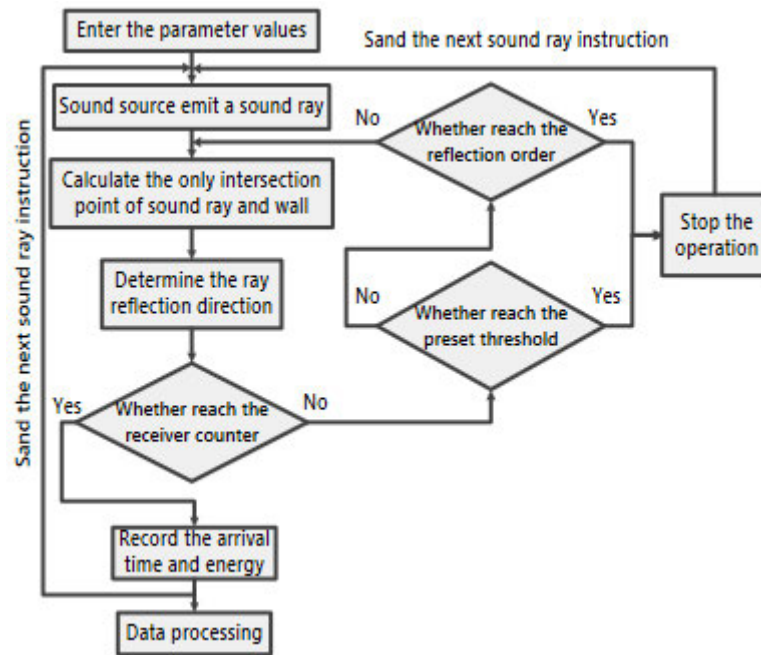


Figure 4-2 Ray-tracing flow chart

After the parameter values have been entered (number of rays, reflection order and reflection time), the ray-tracing simulation starts. The process is simplified in a top-down approach in Figure 4-2. First decision is made after a ray hits any surface for the first time. Here, it will be checked whether the ray hits the receiver. If yes, the arrival time and energy is recorded, if not, it will be checked, if the threshold (defined minimum amount of energy) and afterwards the reflection order is already reached. When both – present threshold and reflection order – are not reached, the process will be repeated for the second hit of the ray for any surface.

5 Application of methodology / contributions

In this chapter, the application of the previously explained Methodology to the use cases with increasing complexity is explained. First, it is shown that the proposed method yields very good results in the context of virtual testing of a generic environment. Subsequently, it is applied to a generic, but real, test space. The core is the application to a model of a very light jet, which has a high complexity in simulation and testing.

5.1 Simulation-based validation of inverse approach

For the simulation based validation of the inverse approach (section 5.1.1), the acoustic model of the semi-anechoic chamber described in section 5.2.1 has been used. A raytracing simulation was performed with a total amount of five million rays to guarantee a good echogram with a sufficient amount of reflections. The energy decay is calculated within the post processing in Matlab and used as an input for the inverse approach to see whether the algorithm is capable of reproducing the energy decay as well as the used material properties. For the simulation based validation, some random absorption for the floor, the walls as well as the ceiling and floor were assumed (0.3 for all one third octave bands and materials).

5.1.1 Results of simulation-based validation of inverse approach

Figure 5-1 shows the energy decay for every one third octave band in the range of 100Hz to 8kHz for the receiver M4 of Figure 5-4. It can be noticed, that the inverse approach is capable of reproducing the energy decay for every one third octave band. For the investigation of the results and the crosscheck whether the programming routine in Matlab is correct, the simulated energy decay was used as an input. These values are given in blue in Figure 5-1. As an initial value for the energy decay a value of 200ms was used. The method is very robust meaning that slight changes in the initial values for the energy decay do not affect the final results. Several variation of start values have been tested.

These initial values are given in black in Figure 5-1. The red line indicates the optimized values as the result of the inverse approach.

In a second step, it was also checked if the inverse approach is capable of reproducing the absorption coefficients of the acoustic model. The results are given in Figure 5-2 and Figure 5-3. The red curve indicates the absorption coefficients of the materials and the grey curve the ones resulting from the inverse approach.

It can be finally noticed, that the inverse approach is also capable of reproducing the absorption coefficients of the materials. In the next step the inverse approach is tested using real measurement data of the energy decay. For this reason the proposed method is validated using numerical testing.

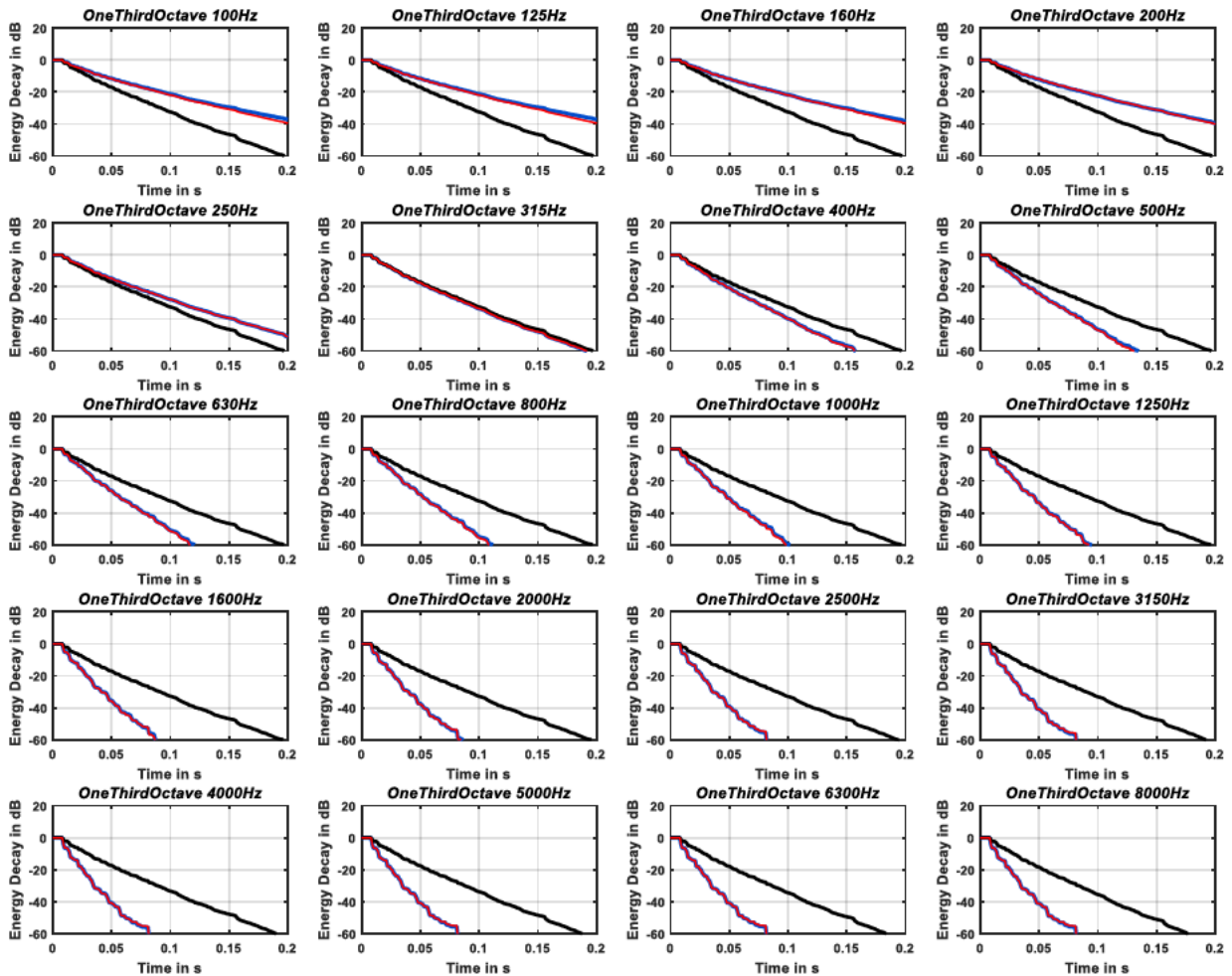


Figure 5-1 simulation based validation of inverse approach for energy decay for receiver M4

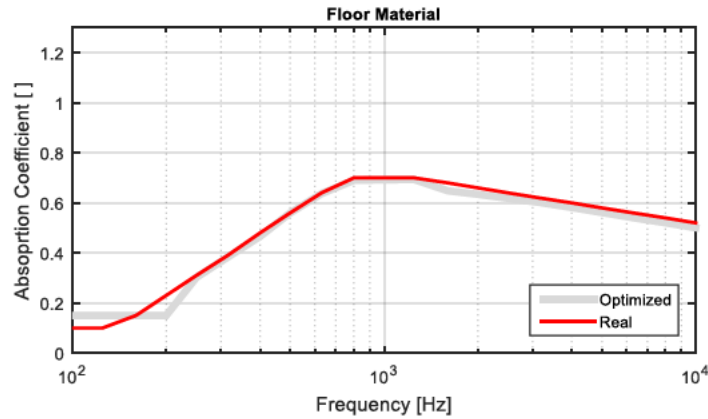


Figure 5-2 simulation based validation of floor absorption

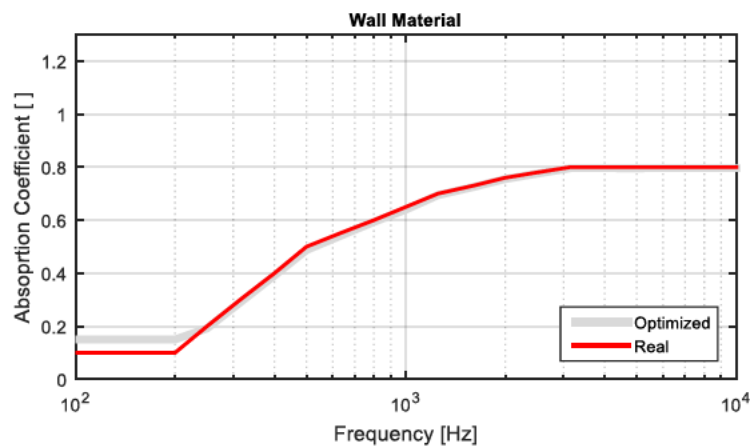


Figure 5-3 simulation based validation of wall absorption

5.2 Simulation of real data – simple use case

5.2.1 Description of test-rig

A semi-anechoic chamber (acoustic EASE Model see Figure 5-4) with dimensions 3.4x3.3x4.5m has been investigated. Photos of the room cannot be shown due to intellectual property rights. Here two different sets of absorption coefficients have been used. The values of the absorption coefficients were obtained from information provided by the supplier of the material. The floor was reflective and the sidewalls as well as the ceiling are made of foam which has an absorption coefficient of 0.9 above 300Hz. One of the four sides (facing the listener position) is normally used as a transmission window and has been blocked up with thick and heavy foam blocks. However, vibro-acoustic coupling with the surrounding laboratory is not completely eliminated. This is a potential source for deviations in the results.

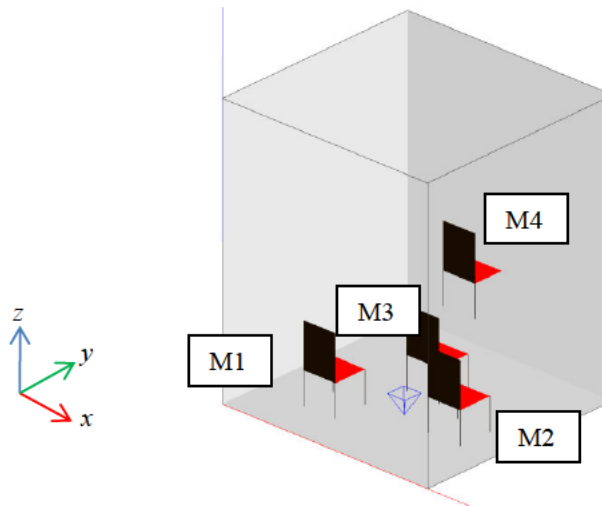


Figure 5-4: acoustic simulation model of simple interior

Within the enclosure, four different measurement positions were defined at positions (x,y,z) and propagation direction. The measurement positions are given in Table 5-1. The rotation (ver, hor and rot) are used for the placement of the listener seats (red/black in Figure 5-4).

Table 5-1 Measurement positions semi-anechoic chamber

	$x[m]$	$y[m]$	$z[m]$	$ver[^\circ]$	$hor[^\circ]$	$rot[^\circ]$
M1_SN2683	1.24	0.75	1.23	0	180	0
M2_SN2680	2.78	1.88	1.13	0	180	0
M3_SN2685	1.97	1.88	1.28	0	180	0
M4_SN2682	1.35	3.22	1.78	0	180	0

5.2.2 Measurement technique and –chain

For the measurement four $\frac{1}{2}$ " diffuse-field microphones manufactured by GRAS (<https://www.gras.dk/> [05/19/2021]) were used (Serial numbers see Table 5-1). The used microphones (Type 46AQ) consist of a preamplifier and a high-precision condenser for general purpose measurements in open acoustic fields. It is a pre-polarized microphone with large dynamic range (3.15Hz to 12.5kHz), a wide frequency range (17 dB(A) to 138dB) and a sensitivity of 50 mV/Pa . This type of microphone is designed for measuring diffuse sound fields. A calibration process was performed for each microphone before starting the measurement. The globe source radiator from Outline (see Figure 5-5) was used as the sound source (sine-sweep, 90.0Hz – 12.5kHz).



Figure 5-5 Globe Source from Outline (<https://www.outline.it/measurement/gsr/index.html> [05/19/2021])

Four separately incoherent noise generators were activated in the globe source to increase homogeneity of the sound field so that the quality of the measurement is improved. The measurement chain is visualized in Figure 5-6. The acoustic behavior of the globe source has also been adapted to the acoustic model (e.g. radiation pattern). An EASE Model of the globe source is provided by the manufacturer Outline.

A voltage data acquisition system (DIC24, manufactured by HEIM) was used for the measurements. It consists of a DC Module capable of measuring 24 channels simultaneously. The module can operate as a standalone front-end (PC connection via USB 2.0) or linked together with additional HEIM DATaRec 4 Modules to a multi-channel system. Each input channel is completely independent and consists of an amplifier, a 24 bit A/D converter and an anti-aliasing filter.

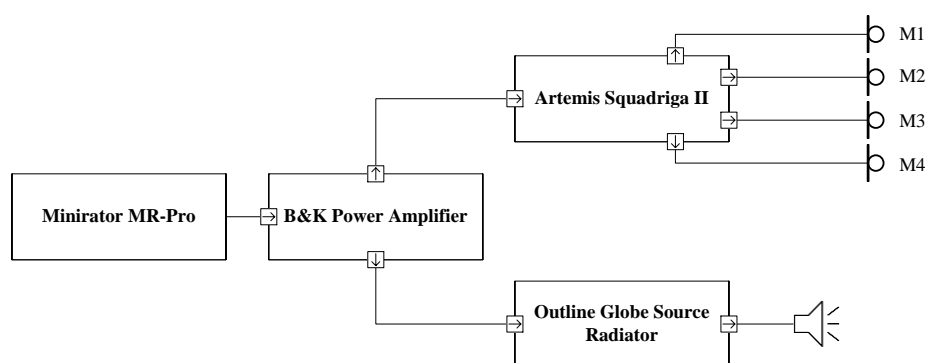


Figure 5-6: measurement chain for simple interior

A sine sweep signal (90 Hz-12.5 kHz) was generated using a Minirator MR-Pro from NTi Audio (<http://www.nti-audio.com/en/products/minirator-mr-pro-mr2.aspx>, [5/19/2022]) and has been used for the measurements. The measurement was performed six times to guarantee a good reproducibility of the measured results. The averaged valued has been used for further investigations.

5.2.3 Results of simple use case

Figure 5-7 shows the energy decay of the microphone position M4 of the semi-anechoic chamber. The results for the microphone positions M1 to M3 can be found in Appendix A. The energy decay was measured using a globe source as described in 5.2.2. The result is given in blue. The energy decay curve gets steeper with an increase in frequency. The inverse approach does not work well in the frequency range of 500Hz, 630Hz and 800Hz. Within these three one third octave bands, the deviation between the measured and the optimized curve is too big (additionally the gradient of the energy decay curve is not steep enough). This might be the case due to some modal behavior within the semi-anechoic chamber. From 1kHz onwards, the gradient of the energy decay is matched very well between measurement and optimization. The deviation is below 2%. The Schroeder frequency of the semi-anechoic room is ~ 200 Hz.

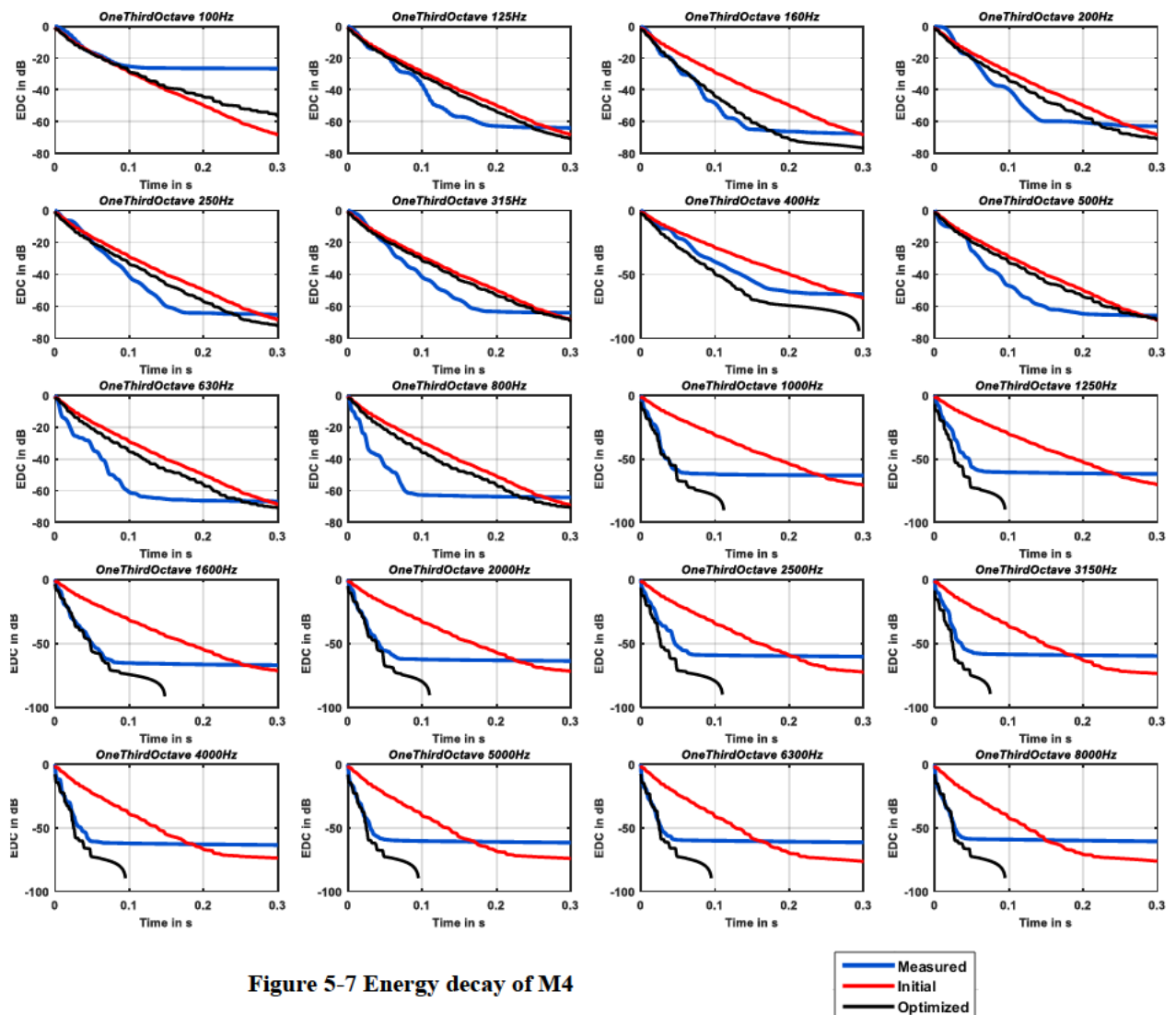


Figure 5-7 Energy decay of M4

Figure 5-8 and Figure 5-9 show the reverberation time T_{30} of the semi-anechoic chamber as well as the result for inverse approach of the optimization algorithm. In the frequency range up to 800 Hz, the optimization result of T_{30} (initial value 0dB) is not in a good agreement with the measurement data. There are certain frequency bands where the error is 30% (e.g. 200Hz). From 800Hz onwards the deviation is small (below 3% deviation) and the optimization routine is capable of reproducing the reverberation time. This is the case because the gradient of the energy decay can be reproduced very well. This is an indicator to see, till what frequency range, a ray tracing model provides good results using the inverse method.

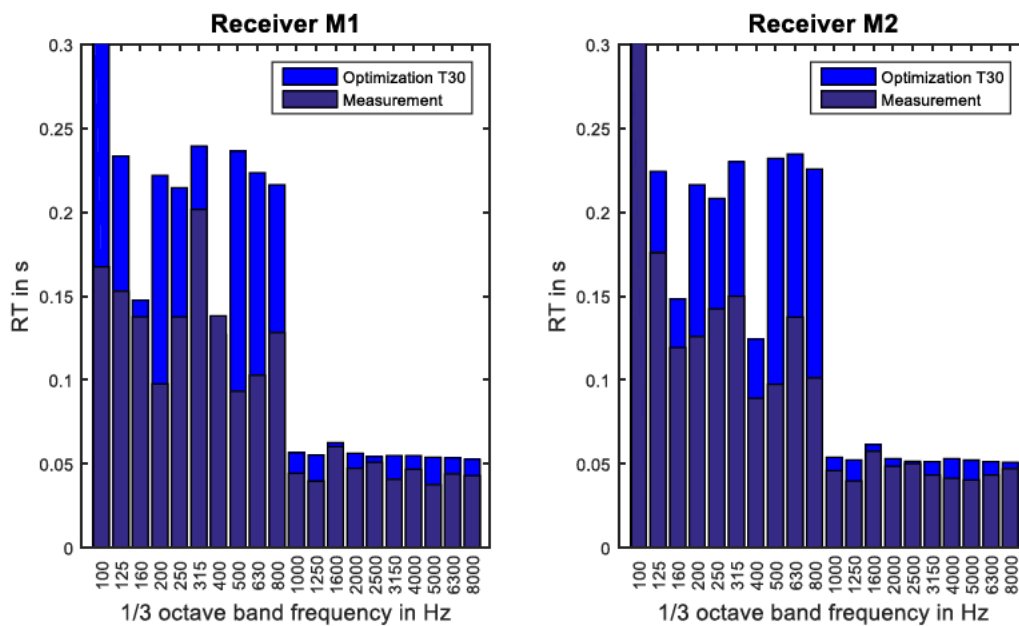


Figure 5-8 Reverberation time semi-anechoic room M1&M2

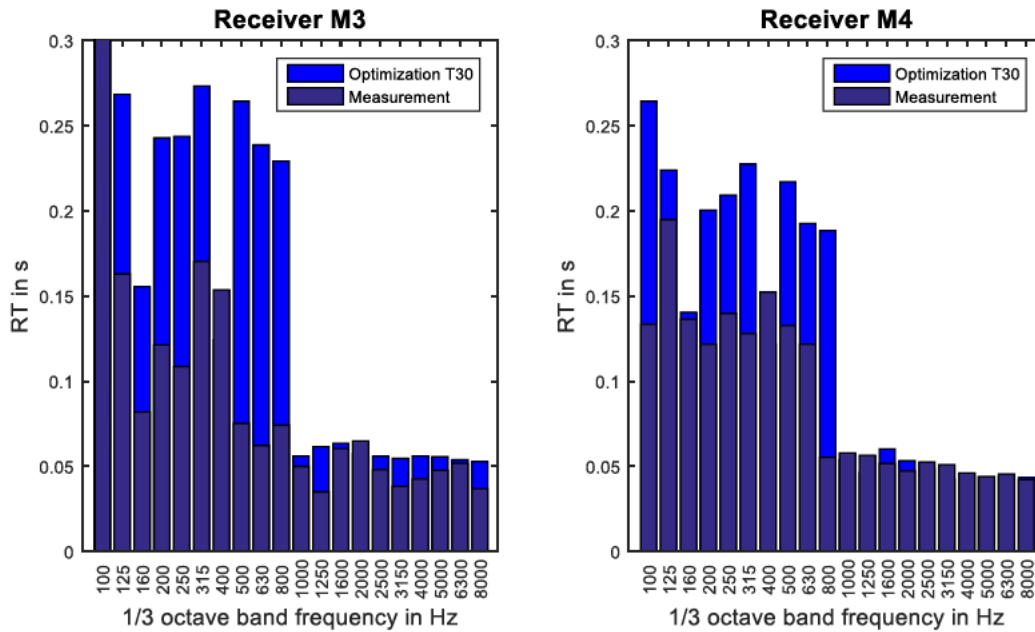


Figure 5-9 Reverberation time semi-anechoic room M3&M4

Figure 5-10 shows the absorption coefficients of the semi-anechoic room. Here, no values are given on the y-axis of the plots due to intellectual property rights. Besides the floor, which is a double wall aluminum structure with foam in between, the room contained three walls (all made out of foam and named Wall1) and one wall of the room which used to be a transmission window to another measurement chamber. This transmission window has been blocked by thick foam blocks. This single wall is called Wall 2 in Figure 5-10. As well as for the reverberation time, it can be noticed, that up to a frequency range of 1kHz the real absorption coefficients coming from the manufacturers documentation have a certain deviation to the ones reproduced by the optimization routine. Due to intellectual property rights of the owner of the test facility, no values are given on the y-axis. For the absorption the same result can be achieved. From 1kHz onwards, the agreement is very good.

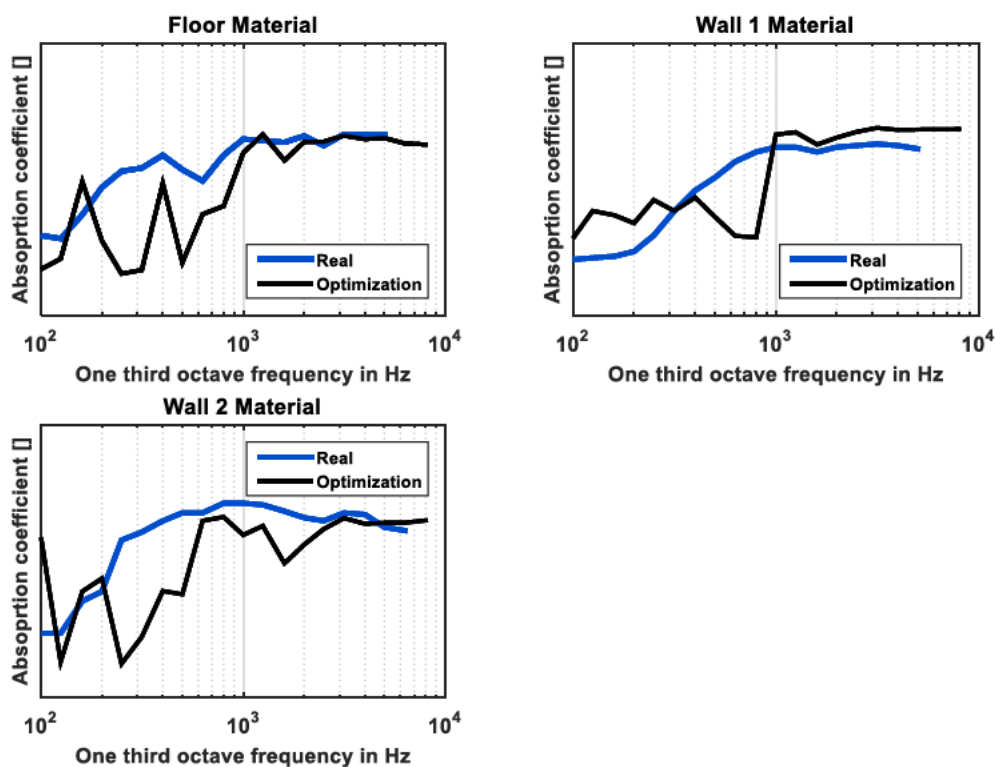


Figure 5-10 Absorption coefficients of semi-anechoic room

Summarizing the analysis of the semi-anechoic chamber as a first simple use case for the inverse approach one can say that the inverse approach can be used till a certain lower boundary in the frequency range, although results in the lower frequency range should be checked with other methods or tools (FEM etc.). As previously described, ray-tracing is not the best method for the lower frequency range.

5.3 Simulation of real data - cabin mock-up

5.3.1 Description of test-rig

The acoustic mock-up (See Figure 5-11) is set up in the Hamburg Center of Aviation Training (HCAT) and is part of the acoustic lab from the University of Applied Sciences Hamburg. The mock-up has been donated by the company Innovint Aircraft Interior GmbH and is referred to a generic commercial business jet. The Interior is equipped with one entrance door to enter the cabin, a seating area of two business seats (left and right) facing each other and a rear partition before the bulk door is closing the cabin mock-up at the rear end. The mock-up itself is build out of wood (very thin lightweight panels) as well as sandwich panels including a honeycomb core. The grey cone at the front representing the cockpit can be disconnected from the cabin part. Windows are also made out of wood. The floor of the cabin part is also equipped with carpet.



Figure 5-11 Mock-up Business Jet at HAW Hamburg

The technical drawing to this cabin is shown in Figure 5-12. The cross-section of the cabin part is shown in Figure 5-13. The part which is investigated is marked with a red dashed line. Both drawings are taken out of the documentation according to the mock-up.

L4). Two of them are located in the ceiling panel (loudspeaker axis facing to the ground) and two of them are located in the partition facing into the cabin.

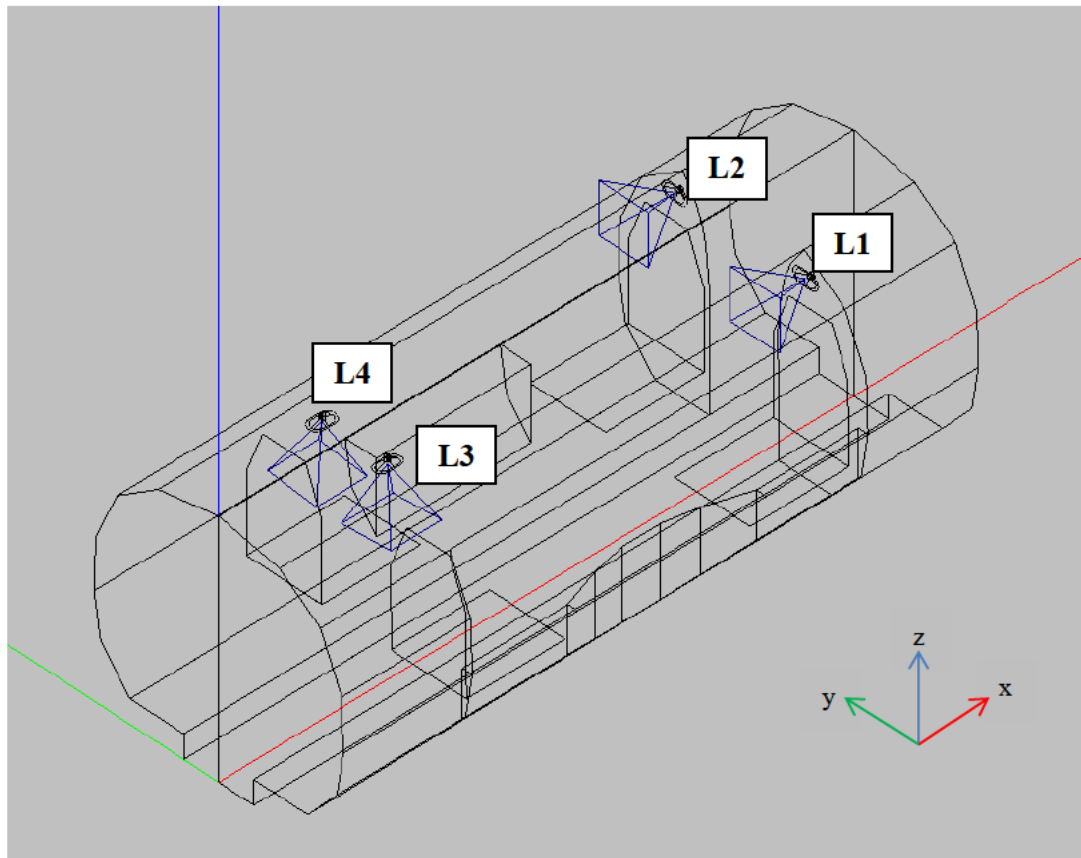


Figure 5-14 Acoustic Model (EASE) of business jet mock-up

5.3.2 Measurement technique and –chain

5.3.2.1 Acoustic properties

To set up the acoustic model properly, different input parameters for the acoustic model are of essential knowledge. The material information (absorption coefficients) is unknown and needed to be measured physically in the mock-up. Here the in situ impedance gun from Microflown has been used which is shown in section 3.2.1. The device can be used in a frequency range of 300Hz to 10kHz and can be used on flat as well as curved surfaces. With a sound source at 23cm from the probe, white noise is generated towards the sample. The sound pressure and the particle velocity are measured at the surface of the material. The design of the impedance gun is equipped with a system to decouple the sensors from the structure born vibration which is generated by the spherical speaker. The absorption and reflection coefficients can be obtained directly from the measured impedance, which is the complex ratio of sound power and particle velocity. For the investigation of the absorption within the mock-up, every material is scanned for a time period of 45 seconds and the measurement is

repeated three times. The repeated measurements are furthermore linear averaged and the averaged absorption curve is used for the input in EASE. The measurement set up files can be found in Appendix B.

For the acoustic simulation of the cabin area a total amount of eight absorption parameters is used and clustered. These absorption coefficients are given in Table 5-2.

Table 5-2 Absorption parameters used in acoustic simulation

Ceiling panel	Partition aft
Sandwich panel	Sidewall pax
Seat backrest back	Seat seating
Seat backrest	Carpet

The result for the measurement of the ceiling panel is given in Figure 5-15. Each measurement has been performed three times. The thick line is the arithmetic mean of the measurements which is used as an input for the simulation. All other measurement can be found in Appendix C. The ceiling panel has not been fully reflective and covered with some cloth at the sealing (also see Figure 5-17).

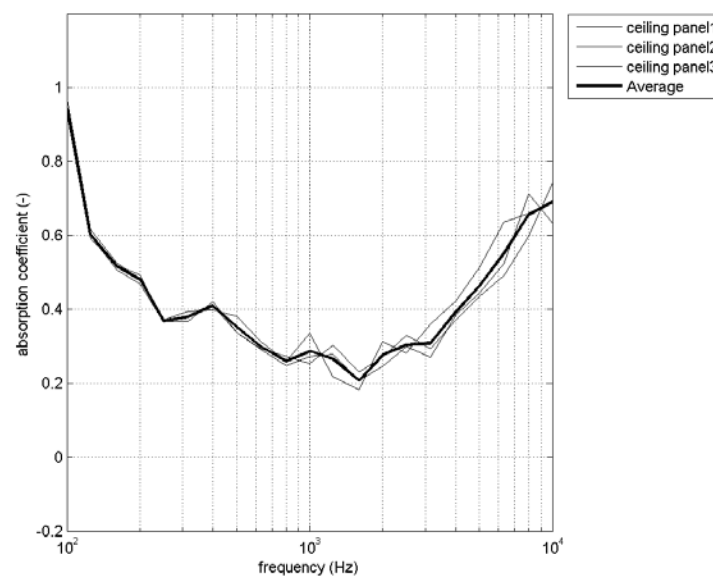


Figure 5-15 Absorption coefficient of ceiling panel in mock-up

The absorption coefficients have been transferred to EASE and used as the input for the simulation (see Figure 5-16).

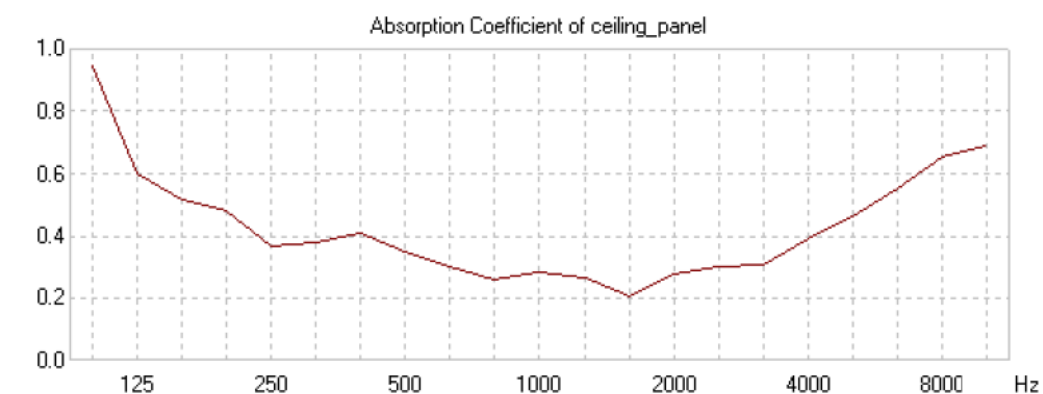


Figure 5-16 Ceiling panel absorption coefficients in EASE

5.3.2.2 Reverberation time measurement mock-up

For the measurement of the reverberation time, the installed four loudspeakers were used (see Figure 5-14). For every loudspeaker two different microphone positions were used. One example is given in Figure 5-17. Two installed loudspeaker in the partition are marked with a yellow square and the measurement microphone from NTi Audio is marked with a green square.

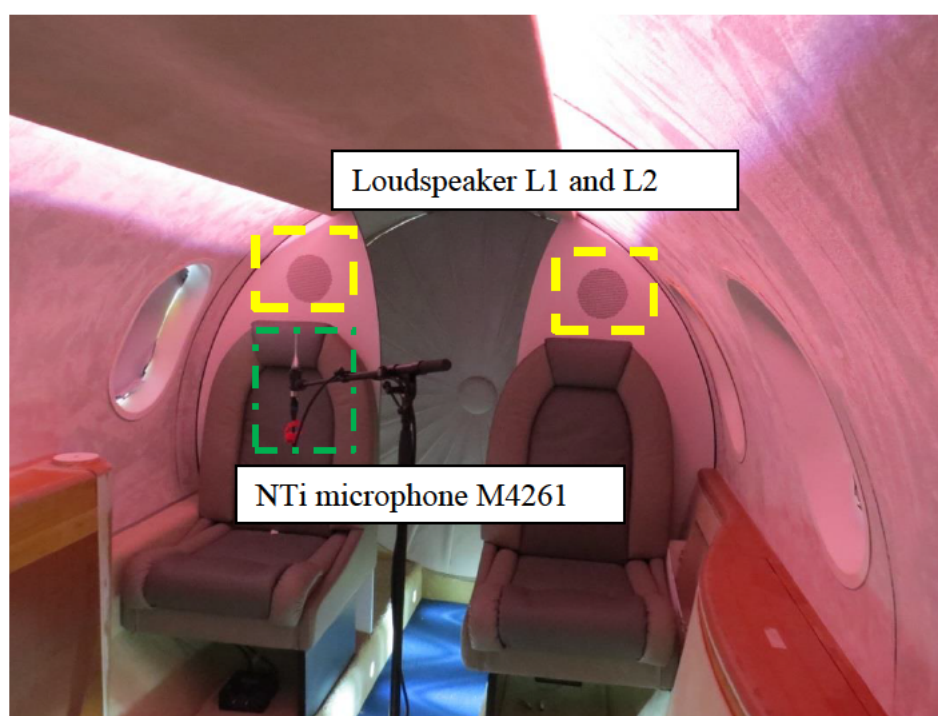


Figure 5-17 Interior of Mock-up, rear end

The measurement was performed using a four channel power amplifier (*Powersoft DIGAM LQ2804*) and a *Fireface UC* as an USB audio interface. This audio system is capable of transferring analog or digital audio data directly to a computer. A class 2 measurement

microphone from NTi Audio (M4261) was used. This microphone is a ¼” microphone with a dynamic range from 27-146dB. EASERA from AFMG was used as the software bundle for the measurements. EASERA (Electronic and Acoustic System Evaluation and Response Analysis) is powerful frond end software which can be run in conjunction to every modern measurement interface. During the measurements, the door was kept closed to ensure no dispersion of sound out of the enclosure. A sine sweep with a range from 100Hz to 12.5kHz was used. It was also ensured, that the frequency range of the sine sweep fits to the capability of the loudspeakers within the mock-up.

Two different microphone positions were investigated for every loudspeaker (L) resulting in a measurement matrix of eight measurements. The positions of the microphones (M) were chosen to cover the volume of the enclosure with emphasis on the seating area. The microphone positions are given in Table 5-3. The coordinate system can be seen in Figure 5-14.

Table 5-3 Microphone positions for reverberation time measurement

		x[m]	y[m]	z[m]
L1	M1	0.33	1.55	1.03
L1	M2	-0.55	2.10	1.03
L2	M3	-0.29	2.21	0.63
L2	M4	0.33	2.24	1.03
L3	M5	0.45	2.66	0.94
L3	M6	-0.55	2.66	0.94
L4	M7	-0.45	2.63	0.95
L4	M8	0.00	2.21	0.63

All eight measurements were analyzed for the reverberation time T_{30} and a frequency range from 100Hz to 10kHz. Figure 5-18 shows the evaluation of the measured data. The measurements have been averaged and plotted. The blue line represents the averaged reverberation time T_{30} for the mock-up. The red and green line represents the minimum and

maximum T_{30} . Due to the dimensions of the enclosure the reverberation time is small with an averaged T_{30} between 11ms to 13ms from 250Hz onwards. The deviation in the lower frequency range is also effected by the location of the mock-up at the acoustic lab at HCAT in Hamburg. Due to the wooden support of the mock-up (see Figure 5-11) as well as the other machines and ventilations running inside the lab, there are some structure- as well as airborne noise effects which interact with the mock-up. With respect to the dimensions of the enclosure and the wavelength of the acoustic waves, one might ask, if the lower frequency range waves can be adequately measured by the microphone. The mock-up is not decoupled (elastic isolation) from modal effects of the laboratory.

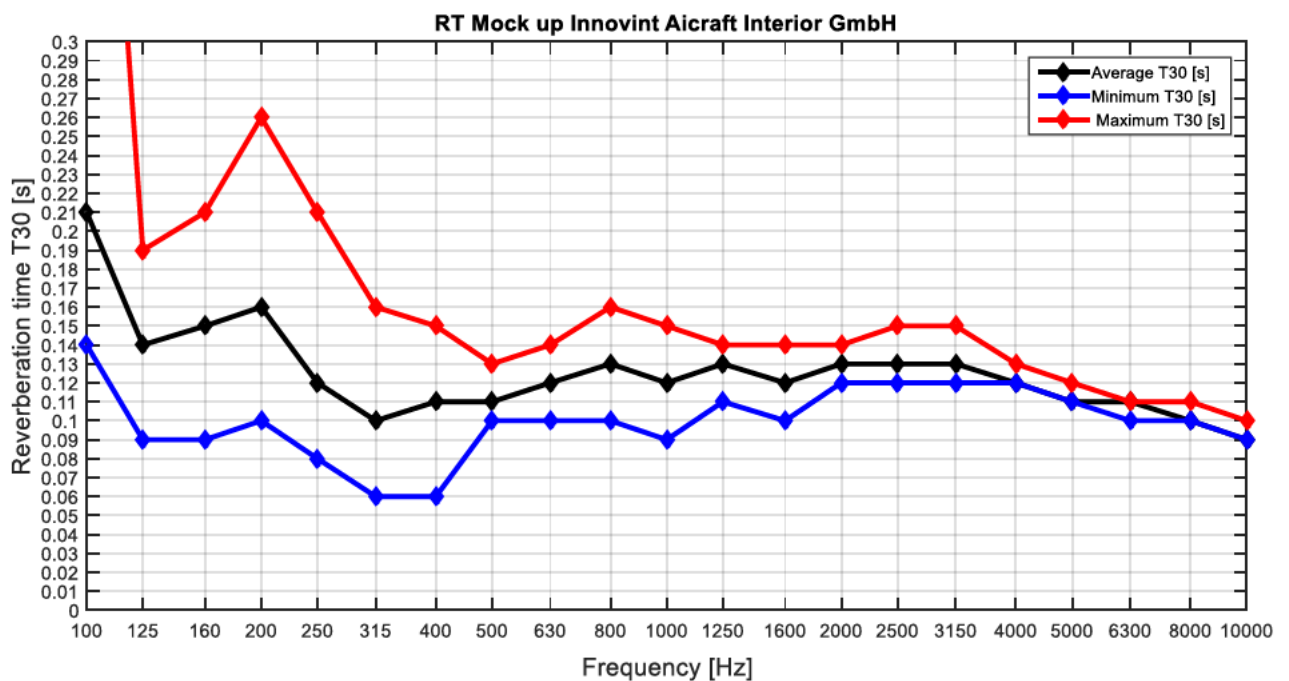


Figure 5-18 Reverberation time T30 for mock-up

5.3.3 Results of real data cabin mock-up

Figure 5-19 shows reverberation time T_{30} of the measurement data (left) and the result of the optimization algorithm (right). The results are averaged for all receiver positions (M1-M8). The starting point for the optimization has been an absorption coefficient of 0.3 for all eight materials in all frequency bands. Figure 5-20 to Figure 5-23 provide detailed information about every receiver position. It can be noticed, that in general the optimized reverberation times are lower than the measured ones. This means that the optimization algorithm predicts more absorption than there certainly is. This means the optimization routine is working on the conservative side for an actual use in an early stage of a new development. The measurement of the reverberation time also includes some uncertainties like transmission of sound from the laboratory into the enclosure.

The result file of the ray tracing simulation of the cabin has been calculated with the following parameters: 500.000Mio rays, a trace control by order 30 and time of 300ms. The calculation time to generate the *Impact file* (filename in EASE) was 5day, 22h and 25minutes (Intel i5 processor).

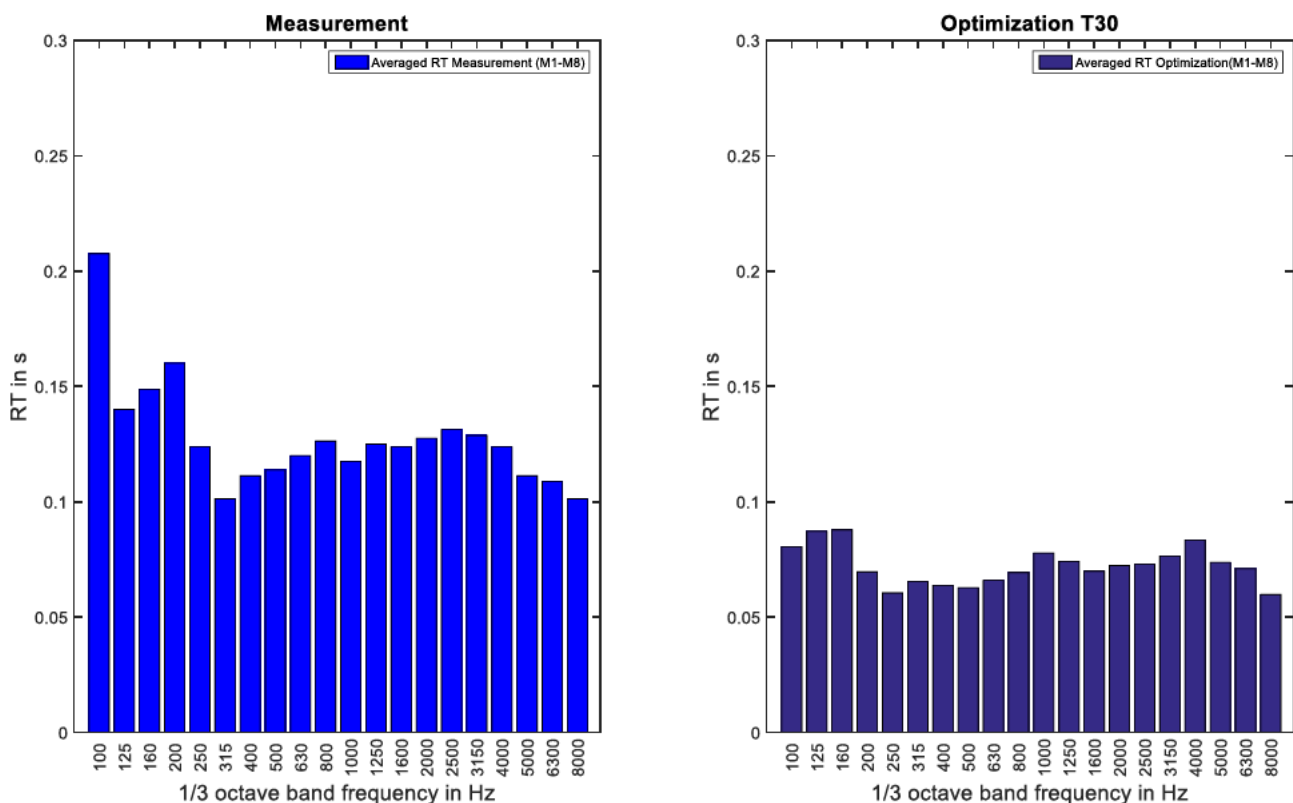


Figure 5-19 Averaged Reverberation Time Measurement (left) and Optimization (right)

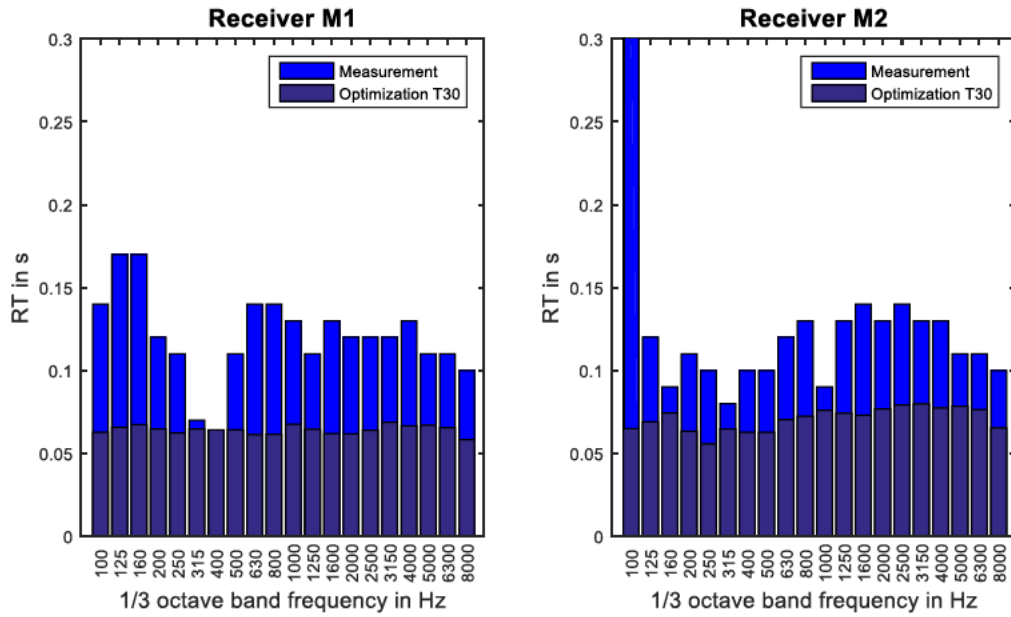


Figure 5-20 Reverberation Time Measurement/Optimization for mock-up M1/M2

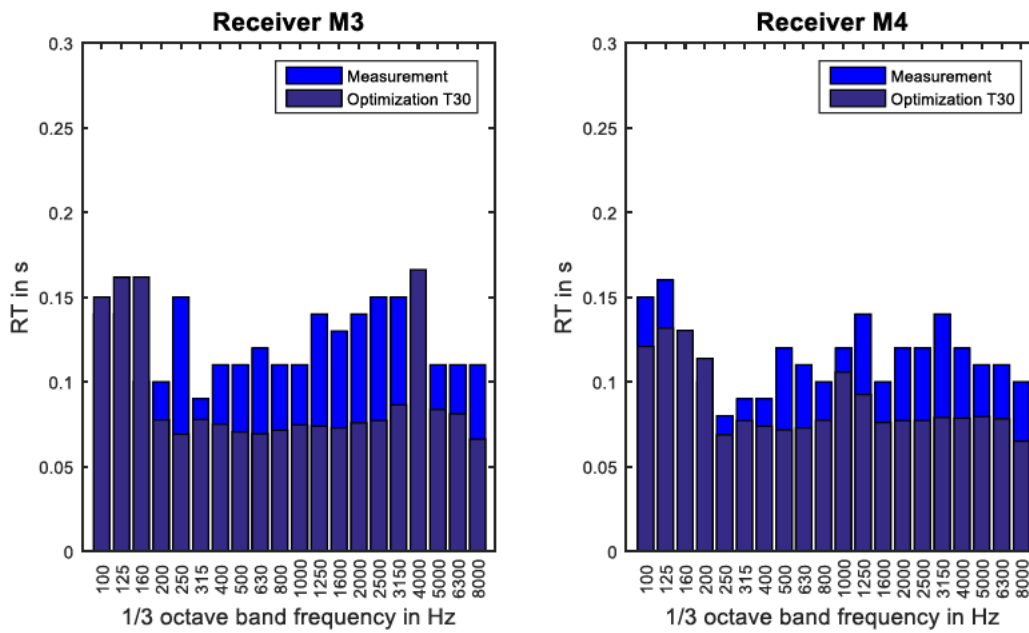


Figure 5-21 Reverberation Time Measurement/Optimization for mock-up M3/M4

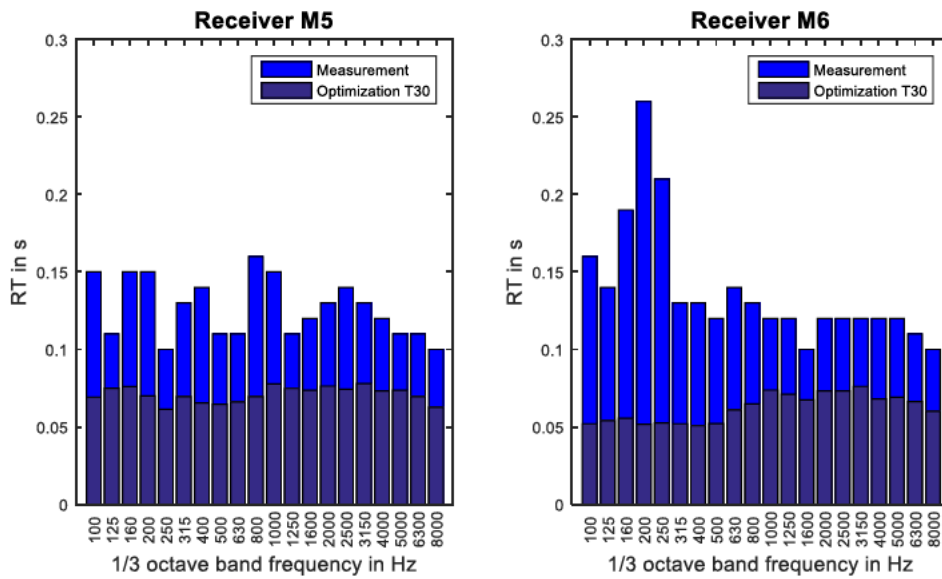


Figure 5-22 Reverberation Time Measurement/Optimization for mock-up M5/M6

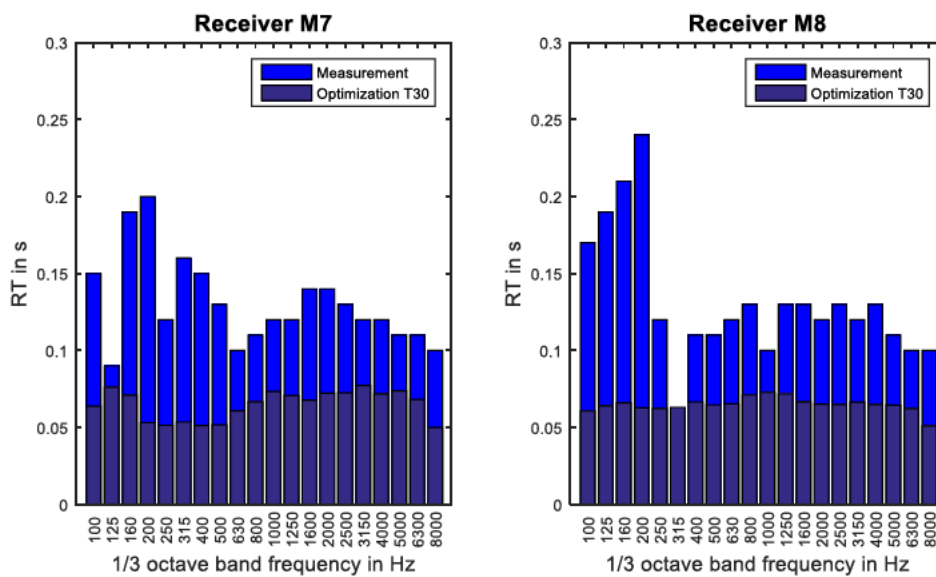


Figure 5-23 Reverberation Time Measurement/Optimization for mock-up M7/M8

Figure 5-24 to Figure 5-27 show the deviation between the measurement and the optimization results. It can be noticed, that the deviation in the lower frequency range is at M5 and M8 comparably high in the low frequency. The prediction of the reverberation time is constantly on the conservative side. This means for practical application that more damping will be added to the cabin which results in a lower noise level. One possible reason for the deviation in the lower frequency range might be modal behavior described in 5.3.2.2.

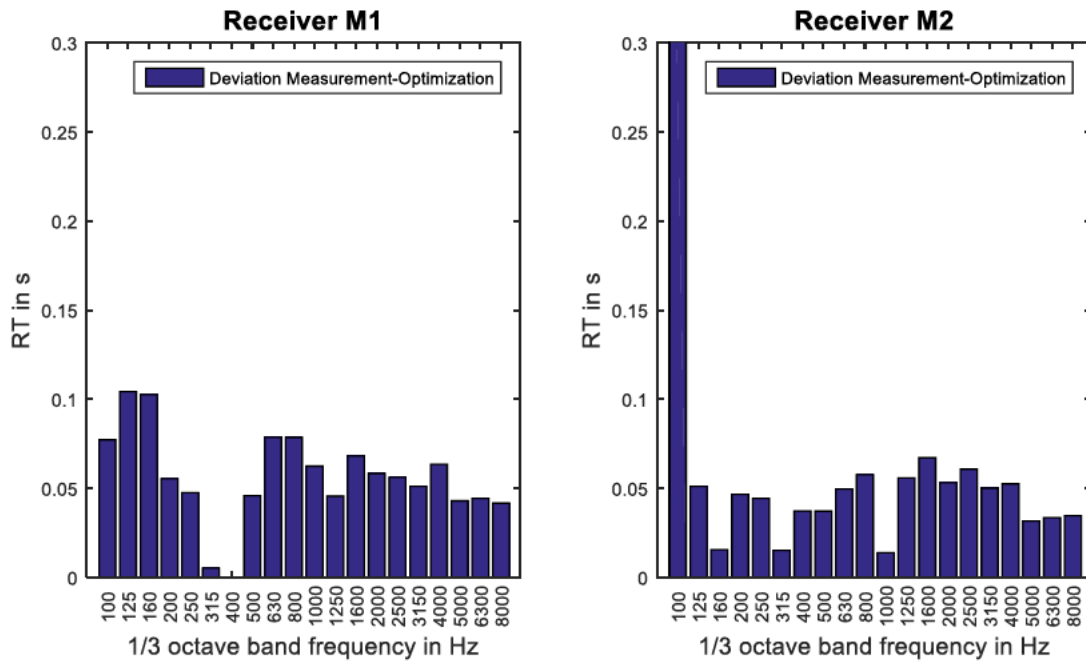


Figure 5-24 Deviation Measurement-Optimization M1/M2

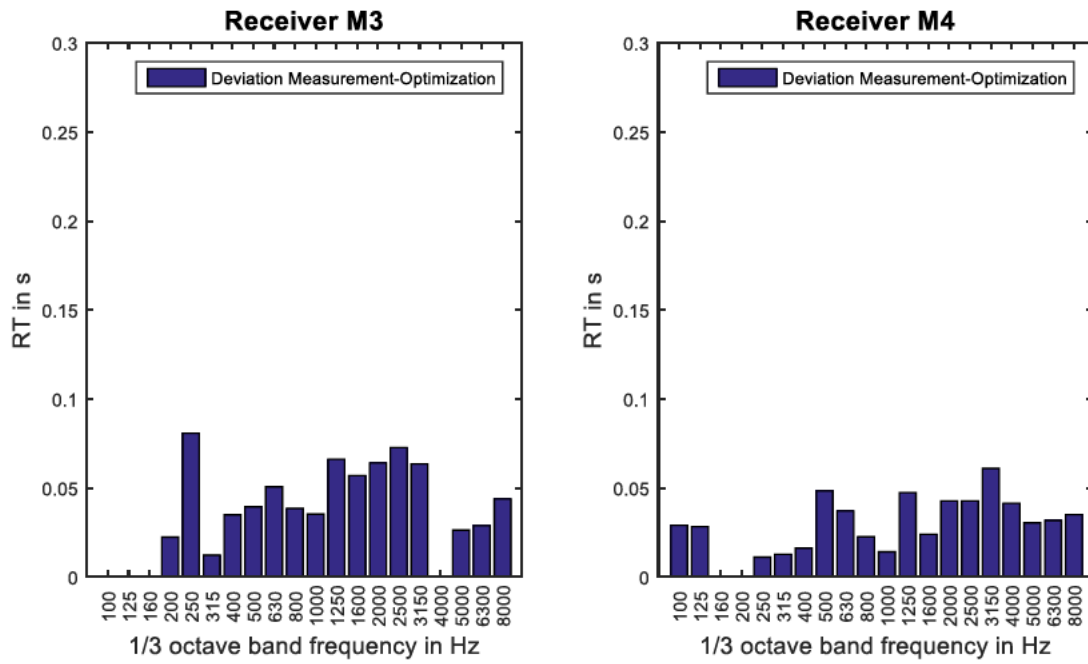


Figure 5-25 Deviation Measurement-Optimization M3/M4

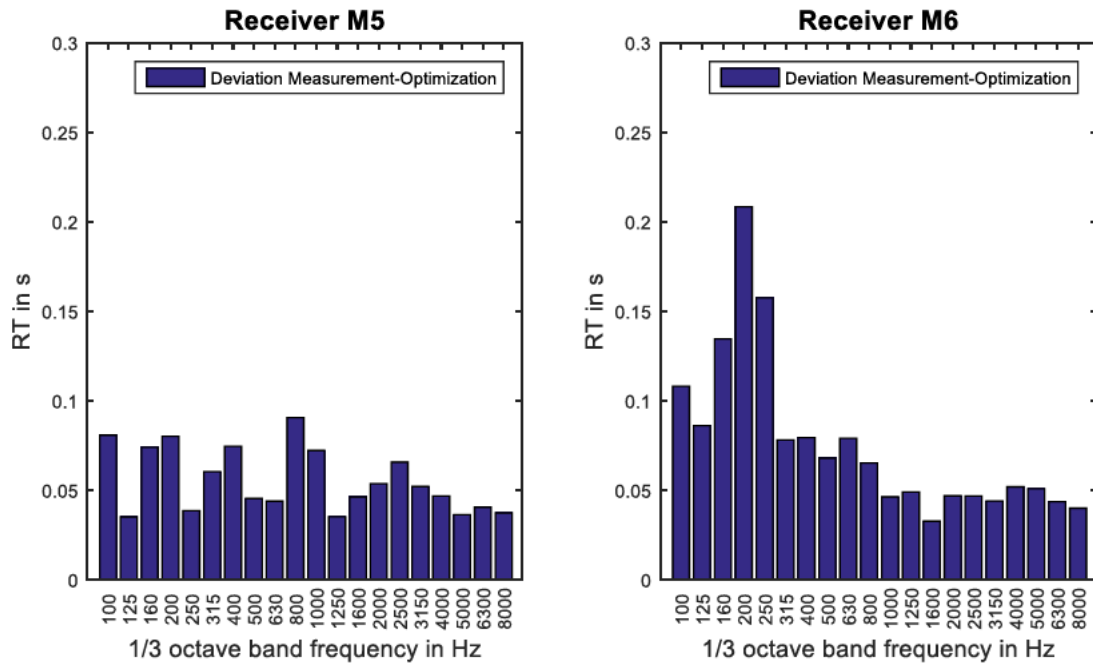


Figure 5-26 Deviation Measurement-Optimization M5/M6

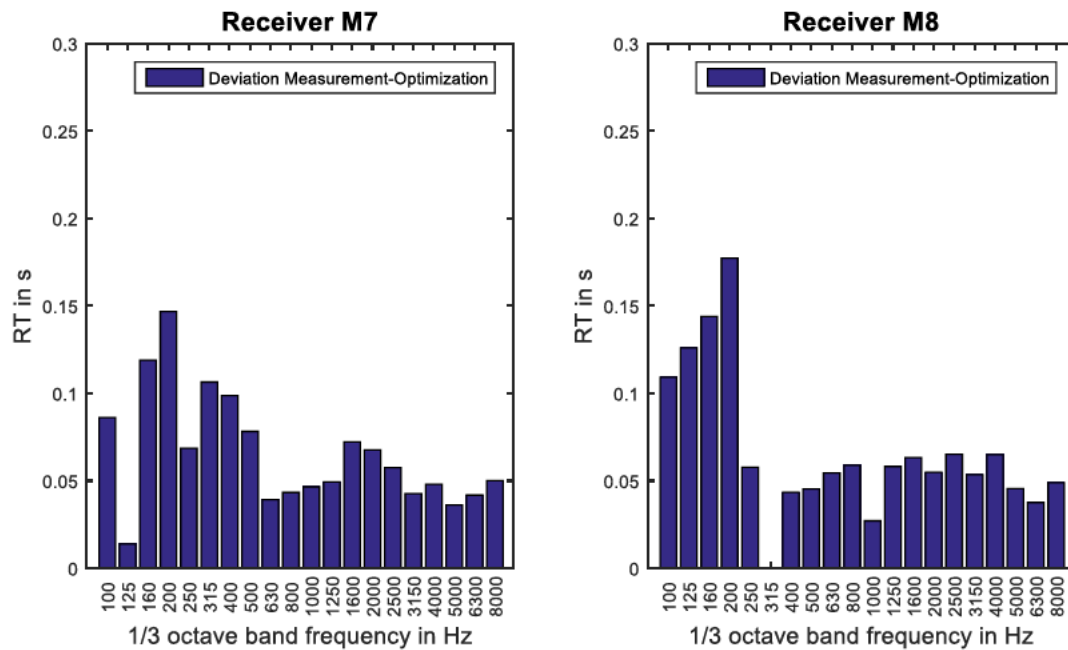


Figure 5-27 Deviation Measurement-Optimization M7/M8

Figure 5-28 to Figure 5-31 show the absorption coefficients for the materials given in Table 5-2. The absorption coefficient for the ceiling panel is in very good agreement with the optimized absorption coefficients based on the ray tracing result of the cabin. Also for the aft partition same trend is reproduced, especially with regards to the frequency bands which are most important for speech intelligibility (500Hz and 2kHz for RASTI). Besides the low

frequency dip for the sidewall pax in the area between 100-160Hz, both sandwich panel and sidewall pax provide the same trend then the measured absorption coefficients (see Figure 5-29).

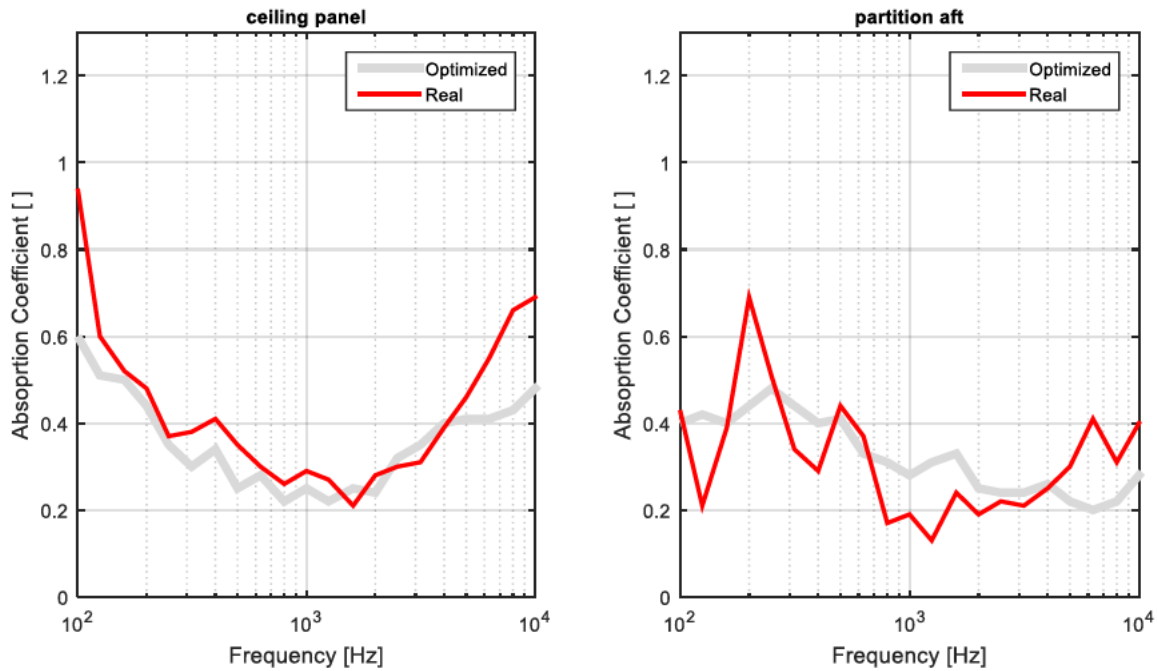


Figure 5-28 Absorption ceiling panel & partition aft

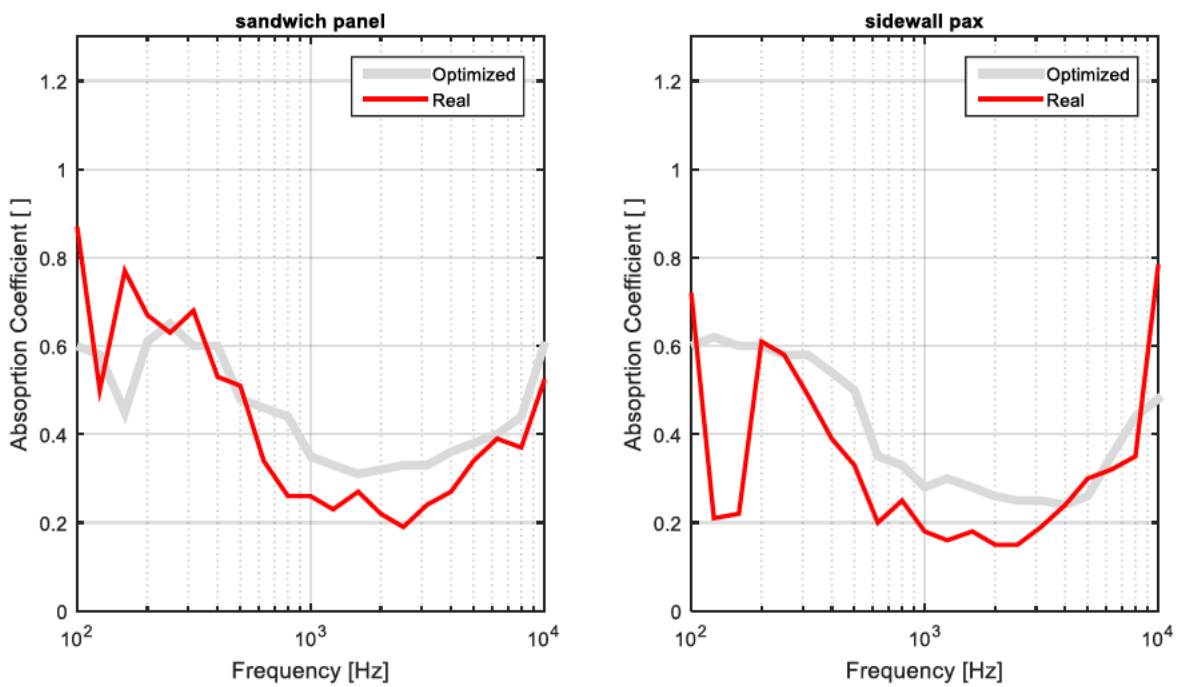


Figure 5-29 Absorption sandwich panel & sidewall pax

For the absorption of the business leather seats, the optimization algorithm provides the same trend although especially in the lower frequency range, the deviation can be up to 40% for seating and backrest. Especially the 800Hz peak for the backrest back is not noticeable in the optimization results. The general trend is plausible for the absorption coefficients of the seat. Although the lower absorption in the lower frequency range of the carpet till 1kHz is 50% over predicted and the trend in the higher frequency range from 1kHz onwards is 20% to low, it can still be used as an input for the acoustic simulation. In general, the trend is reproduced for the various absorption coefficients.

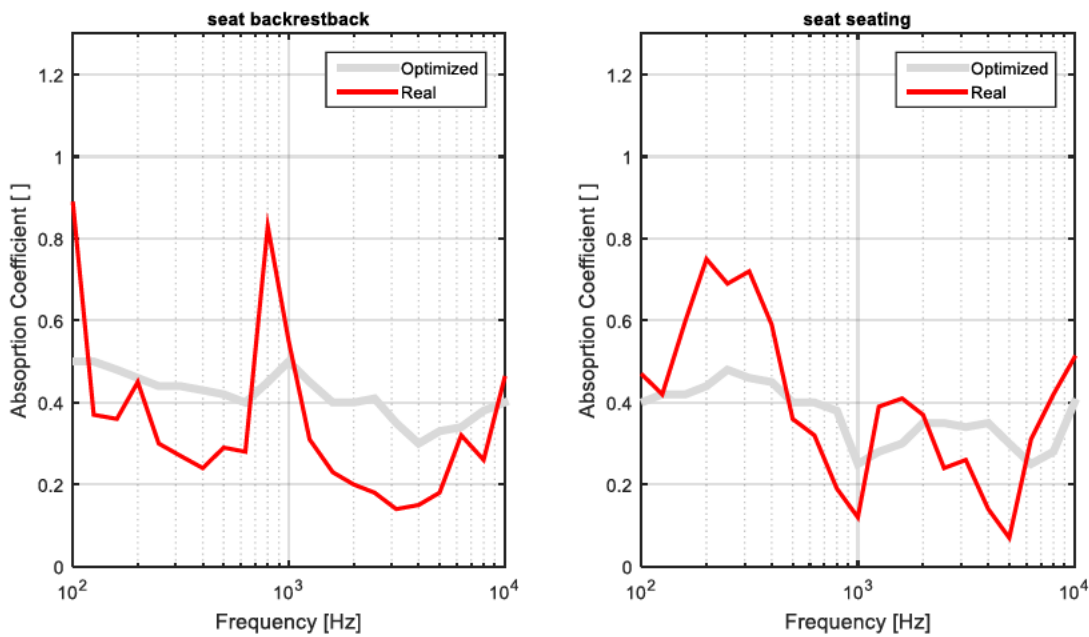


Figure 5-30 Absorption seat backrest back & seat seating

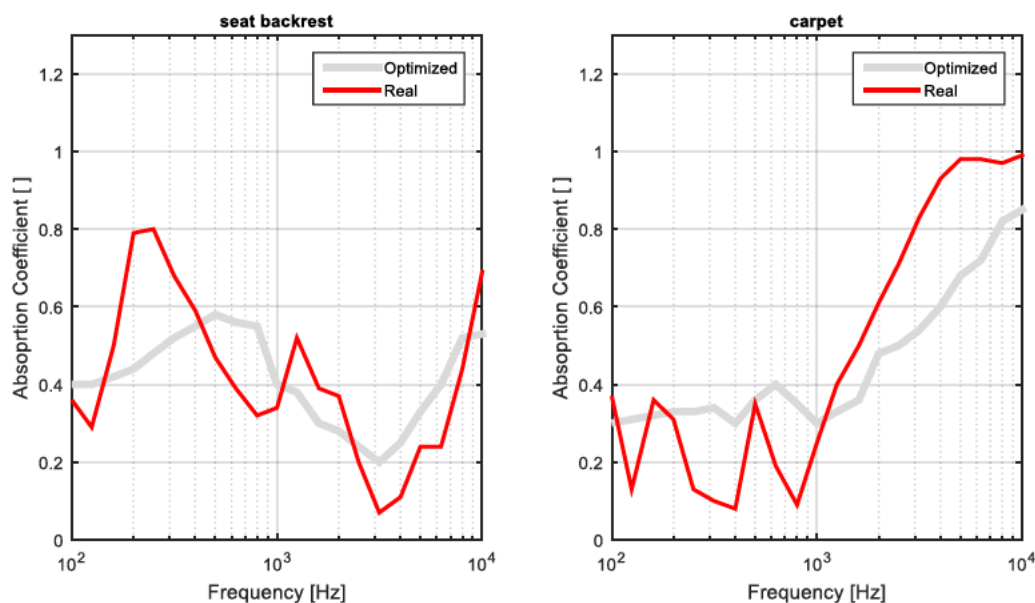


Figure 5-31 Absorption seat backrest & carpet

6 Conclusions & future outlook

The PhD thesis describes an optimization process for absorption coefficients based on an inverse ray tracing method to improve room acoustic simulations of speech transmission intelligibility. At first the inverse approach has been validated for a simple interior, afterwards it is shown that the inverse method can be applied to a complex aircraft cabin and still provides results which improve the quality of the room acoustic model.

For the simple use-case it could be shown that the inverse method is capable of narrowing the measured and simulated energy decay for each of the receiver positions. For the evaluation of the reverberation time especially from 1 kHz onwards, the deviation is below 10%. For the lower frequency range, ray-tracing is not providing good results. This is also known from the literature. With regards to the state of the art and a clear lower boundary for the application of inverse methods based on geometrical acoustics could be identified to 1kHz.

For the complex business jet interior the results show, that the reverberation time can be reproduced by the optimization routine and is still on the conservative side for future developments. The deviation is averaged around 30%. This is mainly the case due to the different boundary conditions. All measurement data needed as input parameters (energy decays and absorption parameters), were measured under laboratory conditions. Vibro-acoustic coupling effects like mounting of the mock-up to the floor or airborne sound transmission from noise inside the laboratory might have affected the measurements. All these effects do not exist in the acoustic simulation, but nevertheless there are good and conservative results. The absorption coefficients provided by the inverse approach generally provide the same trends as the ones which have been measured but still have space to be improved. Especially for the absorption parameters of the ceiling panel the agreement is very good meaning a deviation of max. 10% in the analysed frequency range.

Another contribution to the state of the art is the application of such an inverse method based on geometrical room acoustics on the business jet mock-up. This is a benchmark for future research.

One current problem in the acoustic simulation is that some physical effects such as diffusion and diffraction and also in the lower frequency range the presence of modal behaviour cannot be approximated and are currently not implemented in the software used.

At present due to a convex cost function, the non-linear optimization algorithm LSQnonlin is used and is based on nonlinear least-squares minimization with constraints and is therefore

dependent on the choice of start values. The use of a genetic algorithm therefore offers an approach for improvement.

Within the results of the semi-anechoic chamber as well as for the business jet mock-up it could be noticed, that the deviation in the reverberation time in the frequency range below 800Hz is higher than above. For future improvements, it might be of interest, to use another method for the lower frequency range (e.g. BEM/FEM) to improve the results and couple them to the calculation using ray-tracing which provide good results for the higher frequency range. Thus a hybrid method can be established.

In the next steps, these effects have to be taken into account to also identify absorption coefficients for interiors with high complexity. For interiors with low complexity it is shown, that the optimization routine can be used and also provides plausible and reliable results for the absorption coefficients.

One difficulty of the research work is that in room acoustics and ray-tracing it is always necessary to calculate at least in 2D if not in 3D. Simplifications with 1D approaches are not possible.

For future calculation of trace files when evaluating even more complex structures to reduce the computational time and increase performance, the calculation using GPUs instead of CPUs might be a good approach.

References

- Ali, A., C. Rajakumar, C. & Yunus, S. M., 1995. Advances in acoustic eigenvalue analysis using boundary element method. *Computers & Structures*, pp. pp. 837-847.
- Aoshima, N., 1981. Computer-generated pulse signal applied for sound management. *Journal of the Acoustic Society of America*, 65(5), pp. 1484-1488.
- Aretz, M., 2012. *Combined wave and ray based room acoustic simulations of small rooms*, Aachen: Rheinische-Westfälische Technische Hochschule Aachen.
- Bodén, H. & Abom, M., 1986. Influence of errors on the two-microphone method measuring acoustic properties in ducts. *Journal of the Acoustic Society of America*, 79(2), pp. 541-549.
- Bouhaj, M., Estorff, O. v. & Pfeiffer, A., 2017. An approach for the assessment of the statistical aspects of SEA coupling loss factors and the vibrational energy transmission in complex aircraft structures: experimental investigation and methods benchmark. *Journal of Sound and Vibration*, pp. pp. 152-172.
- Brandao, E., Lenzi, A. & Paul, S., 2015. A review of the in situ impedance and sound absorption measurement techniques. *Acta Acoustica united with Acoustica*, Volume 101, pp. 443-463.
- Burrough, C., Fischer, R. & Rern, F., 1997. An introduction into Statistical Energy Analysis. *Journal of the Acoustic Society of America*, 101(4), pp. 1779-1789.
- Chargin, M. & Gartmeier, O., December 1990. A Finite Element Procedure For Calculating Fluid-Structure Interaction Using MSC/NASTRAN.
- Clough, R.W., 1960. *The Finite Element Methode in Plane Stress Analysis*, Pittsburgh, PA: Proc. 2nd ASCE Conference on Electric Computation.
- Cordioli, J. et al., 2010. On the prediction of damping loss factor of fuselage panels with viscoelastic materials using Periodic Structure Theory and Finite Element Method. *Proceedings of ISMA* , pp. 2257-2266.
- Cox, T. et al., 2006. A Tutorial on Scattering and Diffusion Coefficients for Room Acoustic Surfaces. *Acta Acoustica united with Acoustica*, Volume 92, pp. 1-15.
- Cox, T. & Lam, Y., 1994. Prediction and evaluation of the scattering from quadratic residue diffusors. *Journal of the Acoustic Society of America*, Volume 95, pp. 297-305.
- Cremer, L. & Müller, H., 1982. *Principles of applications of room acoustics*. I & II ed. London: Applied Sciences.
- Culla, A., D'Ambrogio, W., Fragolent, A. & Milana, S., 2016. Vibroacoustic optimization using a statistical energy analysis model. *Journal of Sound and Vibration*, pp. pp. 102-114.
- Dande, H., Wang, T., Maxon, J. & Bouriez, J., 2017. *SEA Model Development for Cabin Noise Prediction of a Large*, s.l.: SAE Technical Paper 2017-01-1764.

- D'Antonio, P. & Konnert, J., 1992. The directional scattering coefficient: Experimental determination. *Journal of the Audio Engineering Society*, Volume 40, pp. 997-1017.
- de Bree, H.-E., 2003. The Microflown: An Acoustic Particle Velocity Sensor. *Acoustics Australia*, 31(3), pp. 91-94.
- Deines, E., 2008. *Acoustic Simulation and Visualization Algorithms*. Kaiserslautern: s.n.
- Deines, E. et al., 2006. Comparative visualization for wave-based and geometrical acoustics. *IEEE Trans. Vis. Comput. Graphics*, Volume vol. 12, no. 5, pp. pp. 1173-1180.
- Denis, V., Pelat, A., Gautier, F. & Elie, B., 2014. Modal Overlap Factor of a beam with an acoustic black hole termination. *Journal of Sound and Vibration*, Issue 333, pp. 2475-2488.
- Ducourneau, J., Faiz, A. & Khanfir, A., 2013. Measuring sound scattering coefficients of uneven surfaces in a reverberant workplace. Principle and validation of method. *Applied Acoustics*, pp. 653-660.
- Dunn, C. & Hawksford, M., 1993. Distortion immunity of mls-derived impulse response measurements. *Audio Engineering Society*, 41(5), pp. 314-335.
- Fahy, F. & Gardoino, P., 2007. *Sound and Structural Vibration*. Oxford: Elsevier.
- Fareed, A., Schmidt, G. & Wahl, F., 2001. Experimental Investigation of Modal Density Parameters of Lightweight Structures. *Technische Mechanik*, pp. pp. 221-225.
- Farina, A., 2000. A new method for measuring the scattering coefficient and the diffusion coefficient of panels. *Acta Acoustica united with Acoustica*, 86(6), pp. 928-942.
- Farina, A., 2000. *Simultaneous measurement of impulse response and distortion with a swept-sine technique*, France: 108th AES Convention.
- Franck, A., 2007. *Energy Finite Element methods for Room Acoustics*. Stuttgart, Germany, s.n.
- Hellemann, J., 2016. *Optimierung von Eingangsgrößen für die raumakustische Simulation unter Berücksichtigung inverser Methoden*, Hamburg: Hochschule für Angewandte Wissenschaften Hamburg.
- Hubbard, H.-H., 1994. *Aeroacoustics of Flight Vehicles: Theory and Practice - Volume 1: Noise Sources*. Hampton, USA: NASA Langley Research Center.
- Hubbard, H.-H., 1994. *Aeroacoustics of Flight Vehicles: Theory and Practice - Volume 2: Noise Control*. Hampton, USA: NASA Langley Research Center.
- IEC 60268-16, 2011. *Elektroakustische Geräte: Teil 16: Objektive Bewertung der Sprachverständlichkeit durch den Sprachübertragungsindex*, s.l.: s.n.
- ISO 10534-1, 2001. *Acoustics - Determination of sound absorption coefficients and impedance in impedance tubes - Part I: Method using standing wave ratio*, s.l.: s.n.

- ISO 10534-2, 2001. *Acoustics - Determination of sound absorption coefficients and impedance in impedance tubes - Part 2: Transfer-function method*, s.l.: s.n.
- ISO 13472-1, 2004. *Akustik - Messung der Schallabsorptionseigenschaften von Straßenoberflächen vor Ort - Teil 1: Freifeldverfahren*, s.l.: s.n.
- ISO 13472-2, 2010. *Akustik - Messung der Schallabsorptionseigenschaften von Straßenoberflächen vor Ort, Teil 2: Impedanzrohrverfahren für reflektierende Oberflächen*, s.l.: s.n.
- ISO 17497-1, 2004. *Acoustics - Sound scattering properties of surfaces - Part I: Measurement of random incidence scattering coefficient in a reverberation room*, s.l.: s.n.
- ISO 17497-2, 2016. *Acoustics - Sound scattering properties of surfaces - Part 2 Measurement of the directional diffusion coefficient in a free field*, s.l.: s.n.
- ISO 18233, 2006. *Akustik - Anwendung neuer Messverfahren in der Bau- und Raumakustik*, s.l.: s.n.
- ISO 3382-2, 2008. *Acoustics - Measurement of parameters in room acoustics - Part 2: Reverberation time in common rooms*, s.l.: s.n.
- ISO 354, 2003. *Acoustics: Measurement of sound absorption in reverberation room*, s.l.: s.n.
- Kletschkowski, T., 2012. *Adaptive Feed-Forward Control of Low Frequency interior Noise*. 1st ed. ed. s.l.: Springer.
- Kletschkowski, T., Weber, M. & Sachau, D., 2011. *Identification of noise sources in an aircraft fuselage structure using an inverse method based on a finite element model*, s.l.: Acta Acoustica united with Acoustica Vol. 97.
- Klos, J. et al., 2005. *Comparison of different measurement techniques for the in-flight assessment of radiated acoustic intensity*, s.l.: Journal of the Acoustic Society of America Vol. 118.
- Knauber, F., Pelzer, S. & Vorländer, M., 2013. *Inverse Ray Tracing for the Optimization of Acoustic Properties in Auralization of real Rooms*, Merano : 39th German annual conference on Acoustics .
- Kopuz, S. & Nalar, N., 1995. Analysis of interior acoustic fields using the finite element method and the boundary element method. *Applied Acoustics*, pp. pp. 193-210.
- Kuipers, E., Wijnant, Y. & de Boer, A., 2012. In situ sound absorption measurement: investigations on oblique incidence. *38th German Annual Conference on Acoustics DAGA*, 19-22 March.
- Kuttruff, H., 2009. *Room Acoustics*. 5th edition ed. Oxon: Spon Press.
- Lanoye, R. et al., 2006. Measuring the free field acoustic impedance and absorption coefficient of sound absorbing materials with a combined particle velocity-pressure sensor. *Journal of the Acoustical Society of America*, Issue 119.

- Lyon, R. & DeJong, R., 1995. *Theory and application of Statistical Energy Analysis*. Boston-USA: Butterworth-Heinemann.
- Mallardo, V., Aliabadi, M., Brancati, A. & Marant, V., 2012. *An accelerated BEM for Simulation of noise control in the aircraft cabin*, s.l.: Aerospace Science and Technology .
- Mankins, J., 2004. *Technology readiness levels*, s.l.: Office of Space Access and Technology NASA.
- Mehre, R. et al., Fe. 2012. An effective GPU-based time domain solver for the acoustic wave equation. *Applied Acoustics*, pp. pp. 83-94.
- Mohammed, Z. & Wang, X., 2016. A deterministic and statistic energy analysis of tyre cavity resonance noise. *Mechanical Systems and Signal Processing*, Issue Vol.70-71, pp. pp. 947-957.
- Mommertz, E. & Vorländer, M., 1995. *Measurement of scattering coefficients of surfaces in the reverberation chamber and free field*, Trondheim: Proc. 15th International Congress on Acoustics (ICA).
- Morkholt, J. & Jacobsen, N.-J., 2004. *Comparison of laser scanning laser measurements and inverse boundary element method*, Dearborn, MI, USA: Proceedings of Conference on Structural Dynamics .
- Nelson, P. & Elliot, S., 1991. *Active Control of Sound*. 1 ed. s.l.:Academic Press.
- Oppenheimer, A., Schaefer, R. & Buck, J. R., 1999. *Discrete-Time Signal Processing*. New Jersey: Prentice-Hall Inc..
- Pelzer, S. & Vorländer, M., 2013. Inversion of a room acoustic model for the determination of acoustical surface properties in enclosed spaces. *The Journal of the Acoustical Society of America*.
- Petrone, G., Melillo, G., Laudiero, A. & de Rosa, S., 2019. A Statistic Energy Analysis (SEA) model of a fuselage section for the prediction of the internal Sound Pressure Level (SPL) at cruise flight condition. *Aerospace Science and Technology*, pp. pp. 340-349.
- Pfeiffer, A., 2016. Full frequency vibro-acoustic simulation in the aeronautic industry. *Proceedings of ISMA* .
- Rienstra, S. & Hirschberg, A., 2004. *An Introduction to Acoustics*. Eindhoven: Eindhoven University of Technology.
- Sadra, D. & Kletschkowski, T., 2016. *Optiomal interior sound management for public and individual transportation systems: Evaluation of objective parameters*, Aachen: 42th German annual conference on Acoustics.
- Sadra, D. & Kletschkowski, T., 2017. *Identification of absorption parameters using an optimization algorithm*, Kiel : 43th German annual conference on Acoustics (DAGA) .
- Savioja, L., 2015. Overview of geometrical room acoustic modeling techniques. *Journal of the Acoustic Society of America*, 138(2), pp. 708-730.

- Schroeder, M., 1979. Integrated-impulse method for measuring sound decay without using impulse. *Journal of the Acoustic Society of America*, 66(2), pp. 497-500.
- Sevgi, L., 2007. Numerical Fourier Transforms: DFT and FFT. *IEEE Antennas and Propagation Magazine*, 49(3), pp. 238-243.
- Stan, G.-B. & Embrechts, J.-J., 2016. *Comparison of different impulse response measurement techniques*, Hamburg: University of Applied Sciences Hamburg.
- Suzuki, Y., Asano, F., Kim, H.-Y. & Sone, T., 1995. An optimum computer-generated pulse signal suitable for the measurement of very long impulse responses. *Journal of the Acoustic Society of America*, 97(2), pp. 1119-1123.
- Thomé, V., 2006. *Galerkin Finite Element Methods for Parabolic problems*. 25 ed. s.l.:Springer.
- Thompson, L., 2006. A review of finite-element methods for time-harmonic acoustics. *Journal of the Acoustic Society of America*, Issue Vol. 119, pp. pp. 1315-1330.
- Tygel, M., Schleicher, J. & Hubral, P., 1994. Kirchhoff-Helmholtz Theory in Modelling and Migration. *Journal of Seismic Exploration*, pp. 203-214.
- Valdivia, N. & Williams, E., 2006. *Study of Comparison of the methods of equivalent sources and boundary element methods for near-field holography*, s.l.: Journal of the Acoustic Society of America Vol. 120.
- Valdivia, N., Williams, E. & Herdic, P., 2008. *Approximations of inverse boundary element methods with partial measurements of pressure sound field*, s.l.: Journal of the Acoustic Society of America.
- Vorländer, M., 1996. *Application of Maximum Length Sequences in Acoustics*, Petrópolis, RJ, Brasil: I Simpósio Brasileiro de Metrologia em Acustica e Vibracoes.
- Vorländer, M., 2008. *Auralization: Fundamentals of Acoustics, Modelling, Simulation, Algorithms and Acoustic Virtual Reality*. Berlin, Germany: Springer.
- Vorländer, M. & Mommertz, E., 2000. Definition of a measurement of random-incidence scattering coefficients. *Applied Acoustics*, Volume 60, pp. 187-199.
- Wandel, M. & Scheel, H., 2016. *Design Requirements of Acoustic Flight LAB Platform*, Hamburg: Proceedings Internoise.
- Williams, E. et al., 2005. *Determination of transmission loss of materials from array measurements using nearfield acoustic holography/inverse boundary element methods in a transmission loss facility*, Minneapolis, USA: Proceedings of Noise-Con..
- Wolkesson, M., 2013. *Evaluation of impedance tube methods - A two microphone in situ method for raod surfaces and the three microphone transfer function method for porous materials*, Sweden: Chalmers University of Technology.

Wu, Y., Fu, Z. & Min, J., 2022. *A modified formulation of singular boundary method for exterior acoustics*, s.l.: Tech Science Press.

Ye, Y. & Fu, Q., 2014. Studies on the Accuracy of Acoustic Simulation based on EASE Software. *IEEE International Conference on Progress in Informatics and Computing*, pp. 242-246.

Zienkiewicz, O. & Taylor, R. L., 2000. *The Finite Element Method*. 5th ed. ed. Oxford, UK: Butterworth-Heinemann.

Appendix A – Energy decay curves for semi-anechoic chamber

Figure A-1 to Figure A-3 show the energy decay curve as a result for the semi-anechoic chamber.

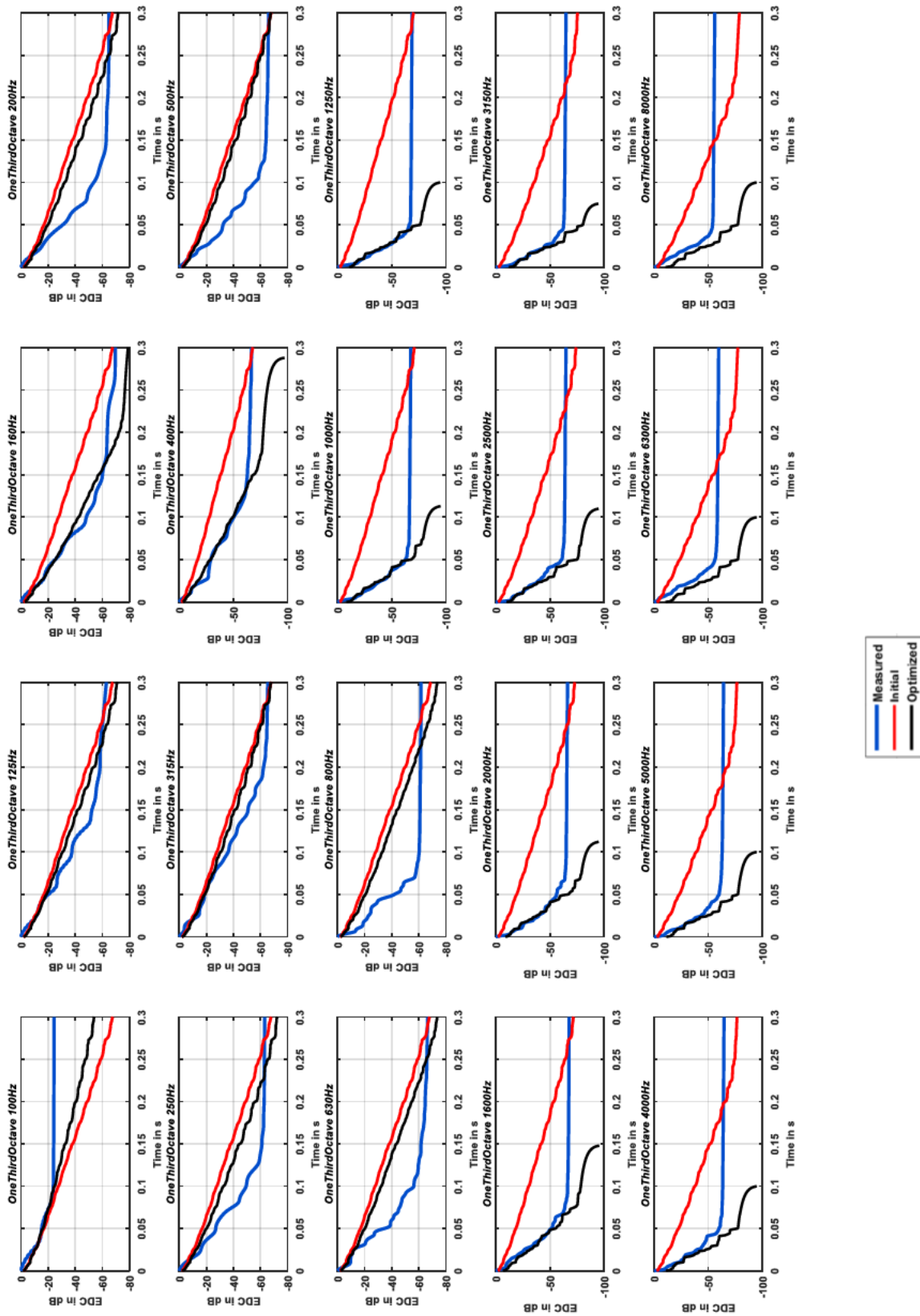


Figure A-1 Energy decay curve M1

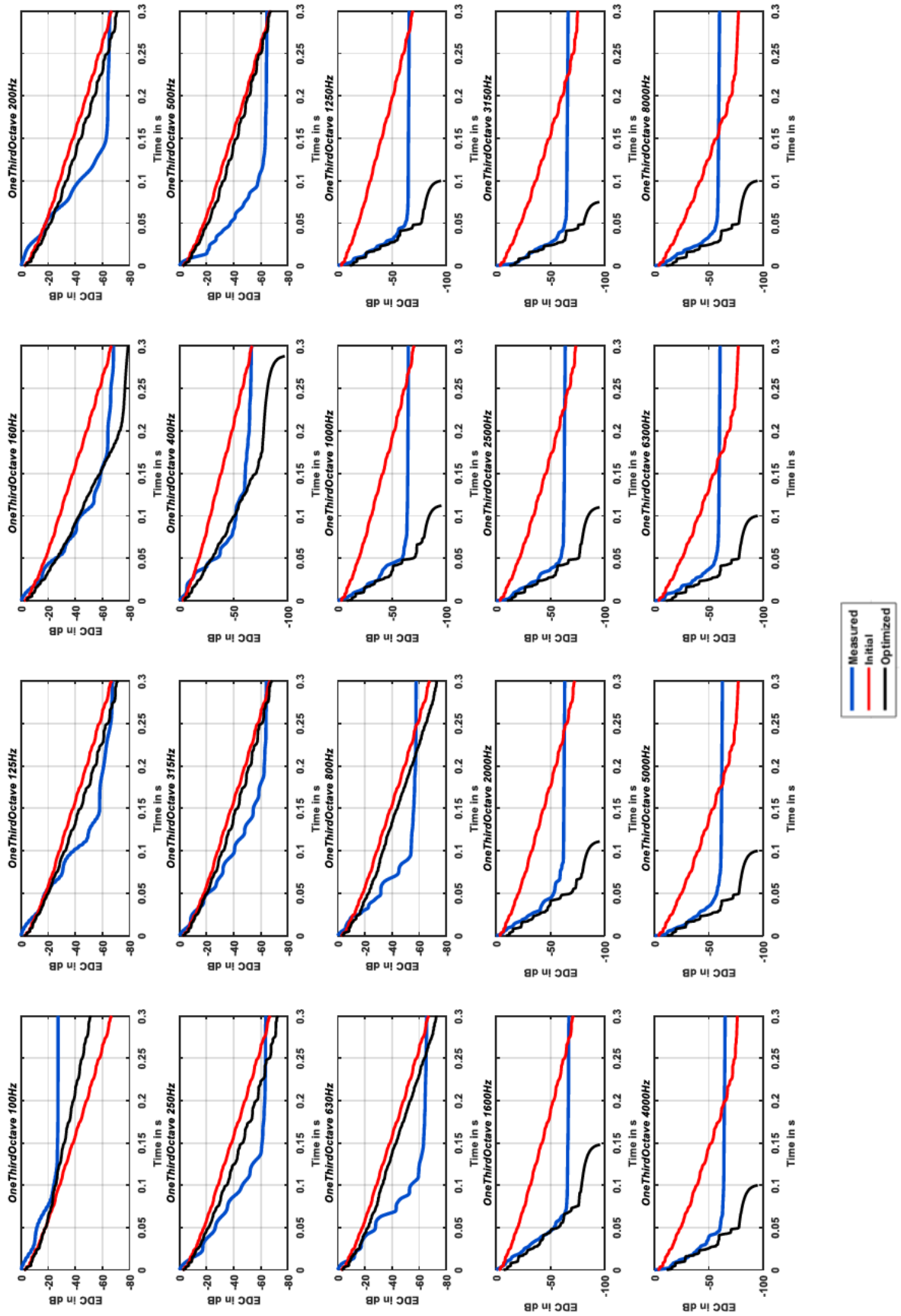


Figure A-2 Energy decay curve M2

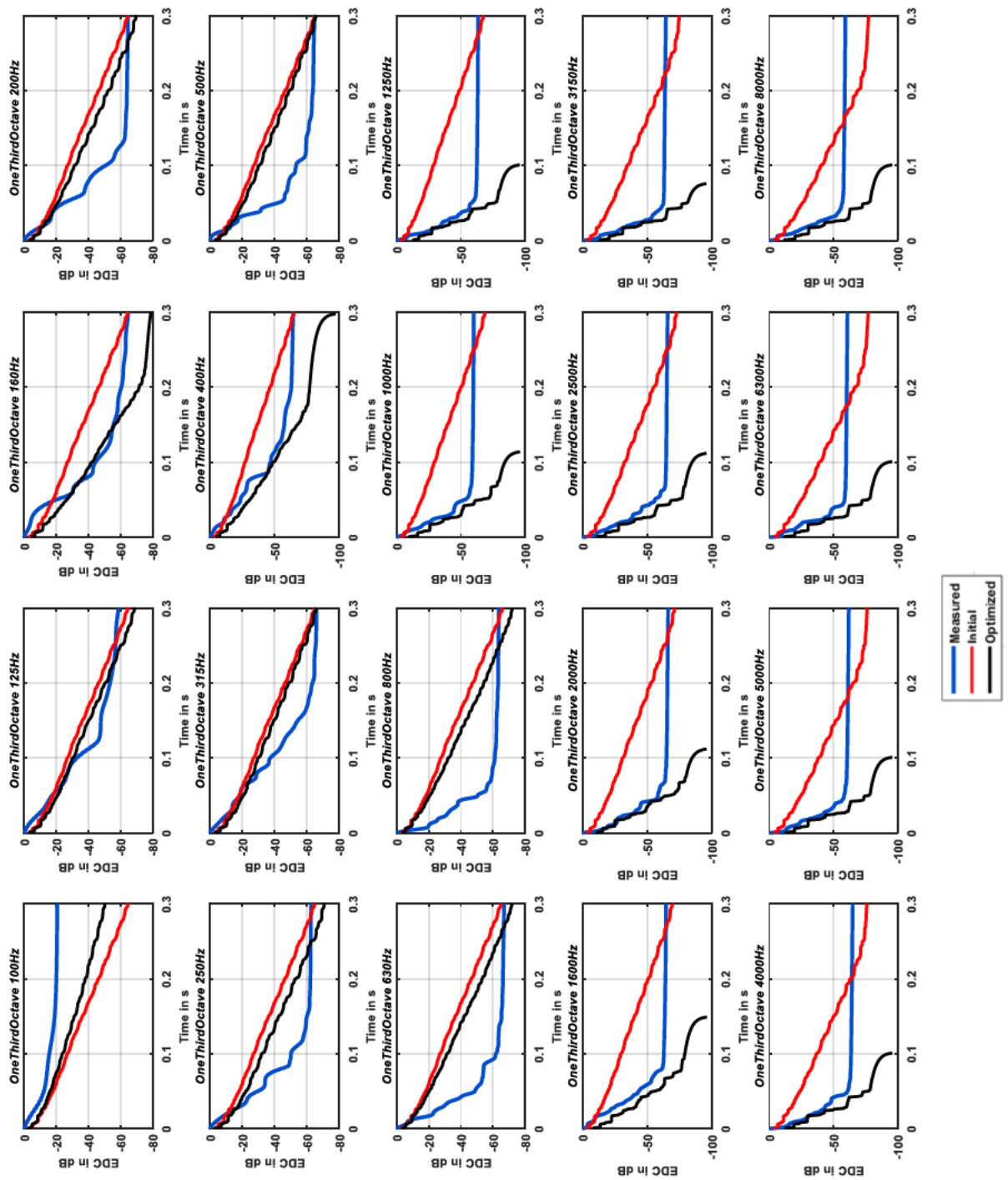


Figure A-3 Energy decay curve M3

Appendix B – Setup files absorption measurement

For the measurement of the absorption coefficients using the Microflown impedance gun, global settings as well as the coefficient calibration of the PU sensor is necessary. The used settings are shown in Figure B-1 to Figure B-3.

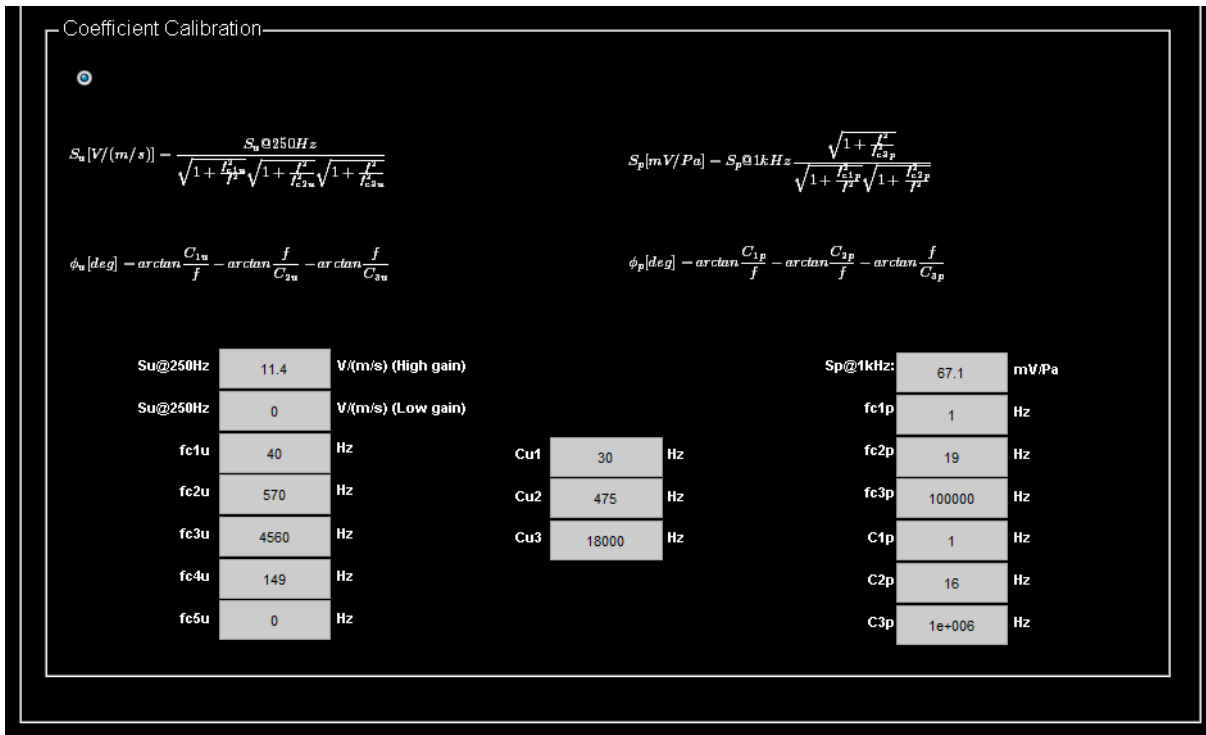


Figure B-1 Coefficient calibration of PU sensor

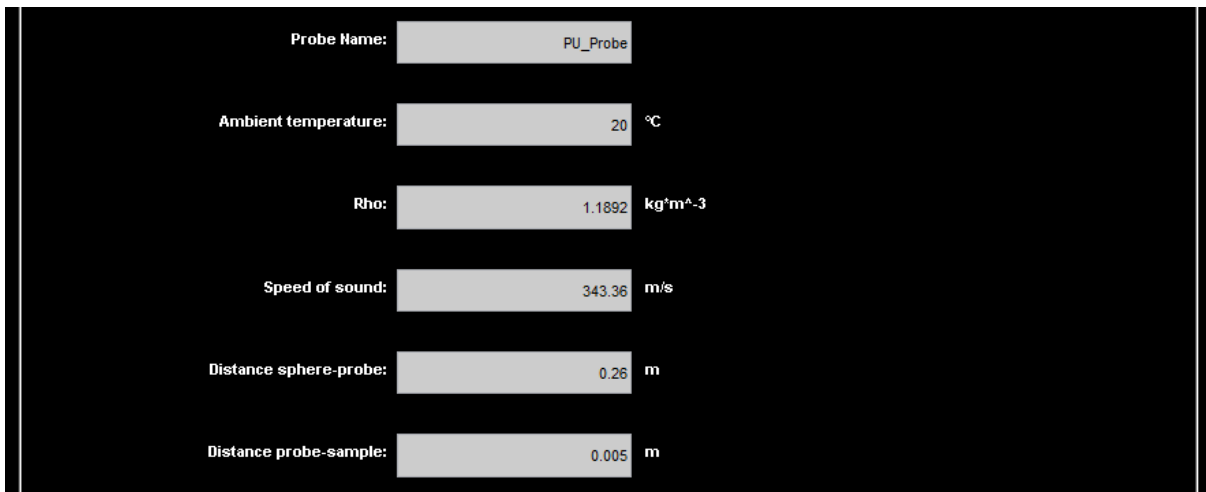


Figure B-2 Global Settings of Microflown Impedance gun measurement (1)

The image shows a software interface with two main sections: Global Settings and Acquisition Settings.

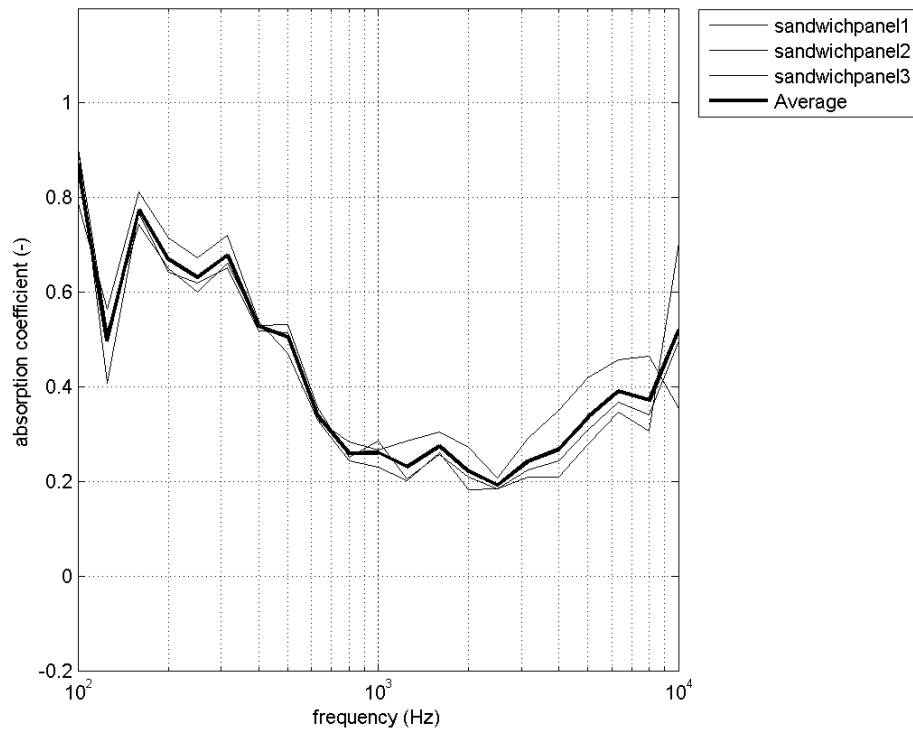
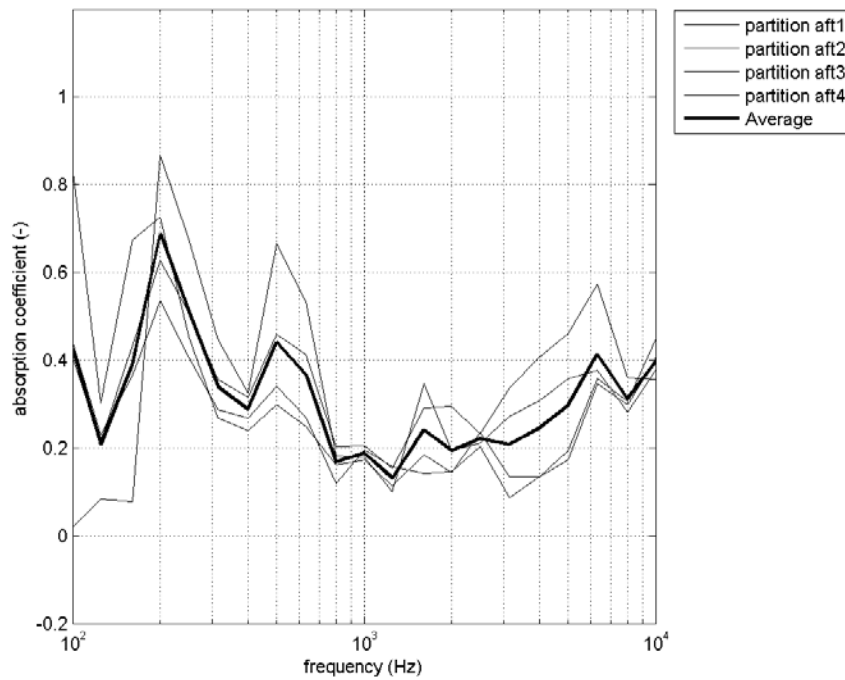
Global Settings:

- Default Calibration Path: C:\Users\Public\Microflow\Imp\Impedance 3.2\Calibration
- Default Measurement Path: C:\Users\Public\Microflow\Imp\Impedance 3.2\Measurements
- Default Project Path: C:\Users\Public\Microflow\Imp\Impedance 3.2\Projects
- Probe Name: PU_Probe
- Ambient temperature: 20 °C
- Rho: 1.1892 kg/m³
- Speed of sound: 343.36 m/s
- Distance sphere-probe: 0.26 m
- Distance probe-sample: 0.005 m

Acquisition Settings:

- Sample Rate: 48000
- Input adapter: dtol
- Input ID: 0
- Input: 0-1
- DT9837-A(00) : DT9837-A
- Calibrate Input (button)
- Output adapter: dtol
- Output ID: 0
- DT9837-A(00) : DT9837-A

Figure B-3 Global Settings of Microflow Impedance gun measurement (2)

Appendix C – Plots of Absorption Measurement in Mock-Up**Figure C-1 Measured Absorption for sandwich panel****Figure C-2 Measured Absorption for partition aft**

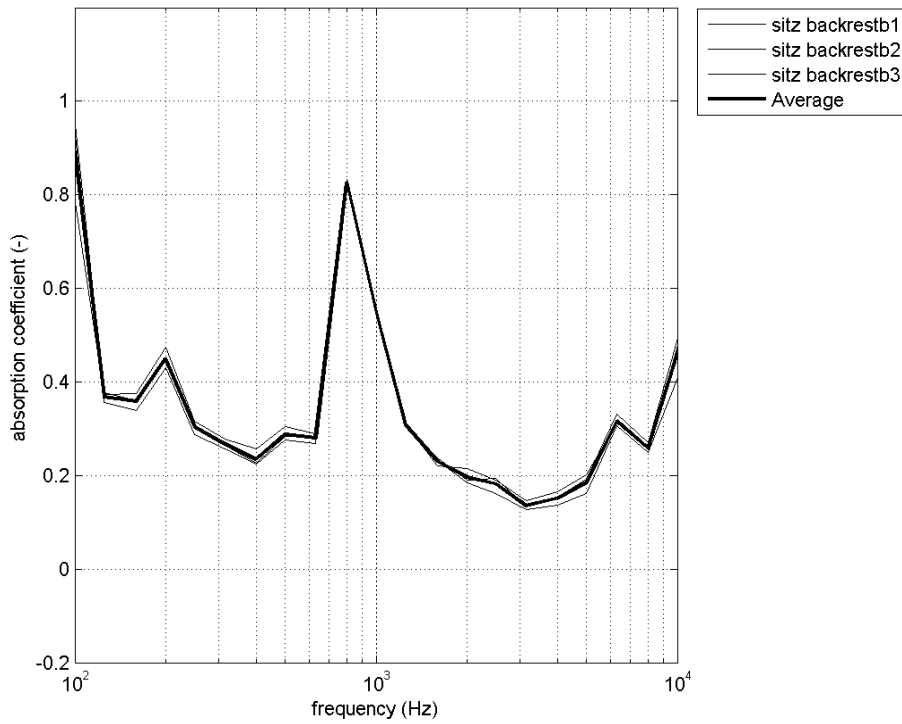


Figure C-3 Measured Absorption seat backrest back

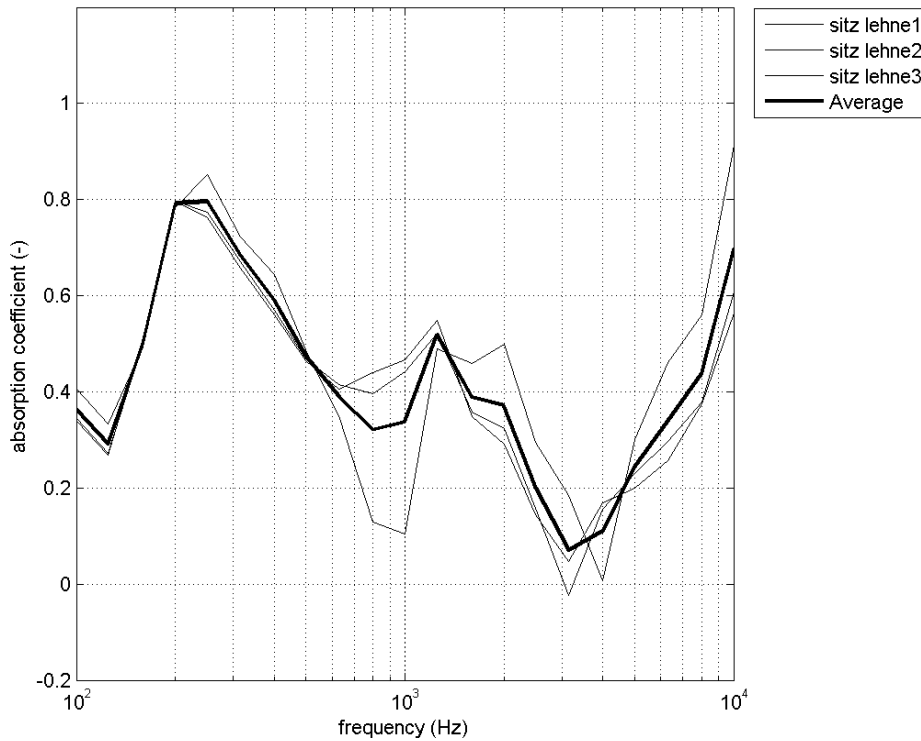


Figure C-4 Measured Absorption for seat backrest

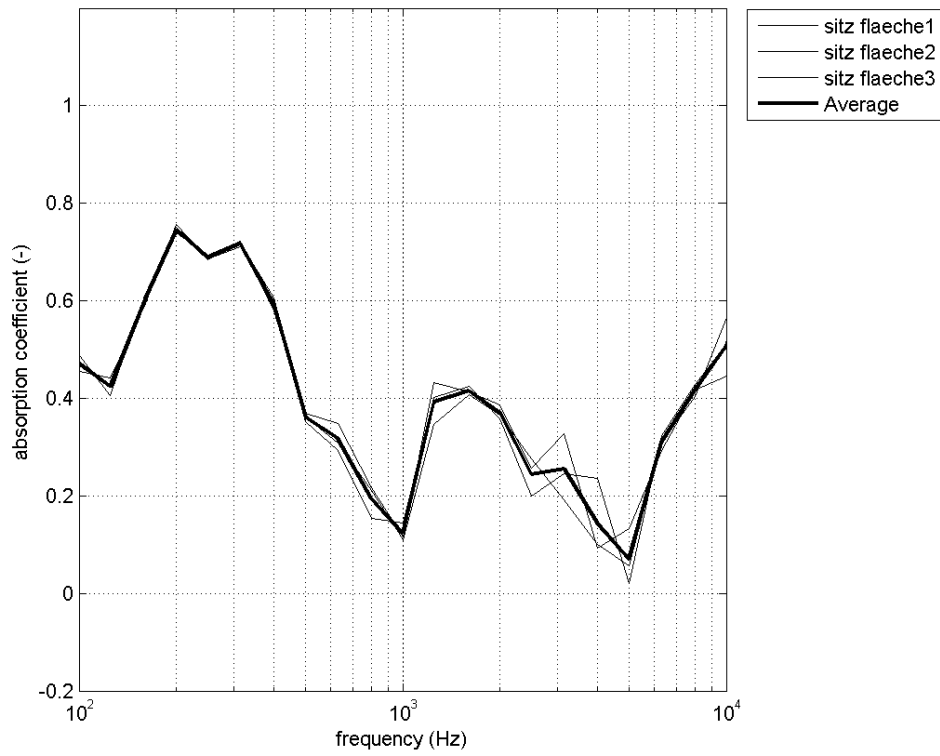


Figure C-5 Measured Absorption seat seating

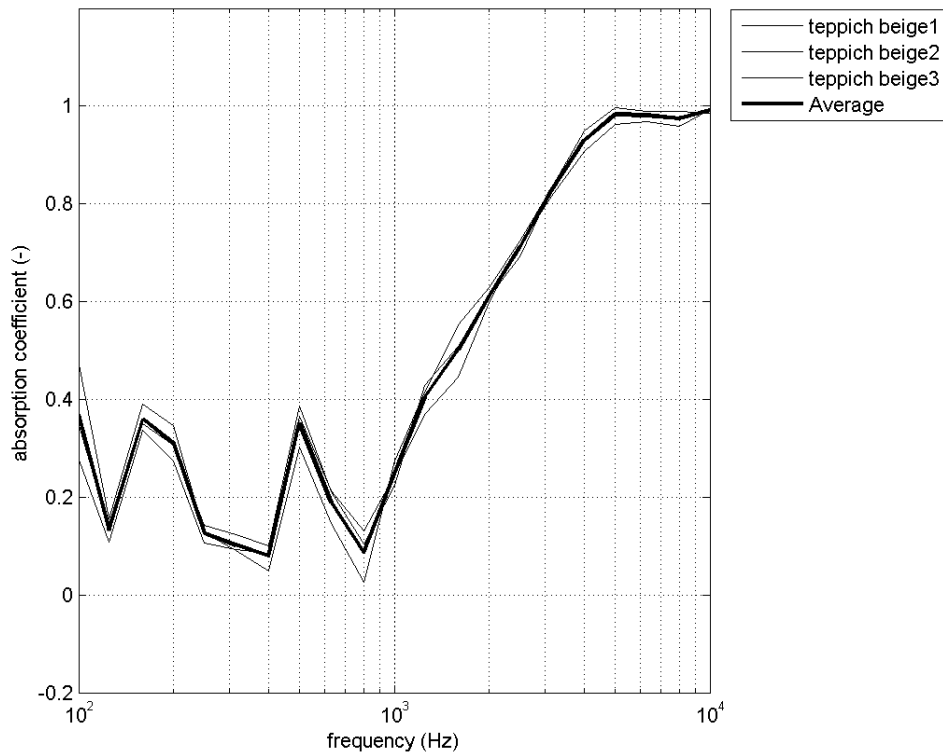


Figure C-6 Measured Absorption carpet

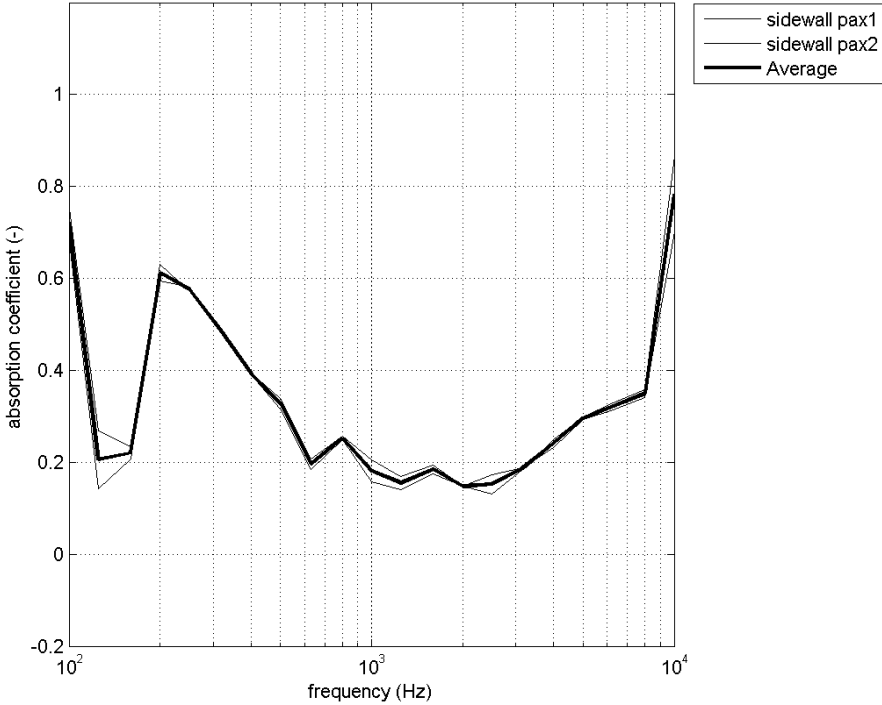


Figure C-7 Measured Absorption sidewall pax